2.7. Human livers and preparation of microsomes and total RNA

Human liver samples from 15 donors were obtained from Human and Animal Bridging (HAB) Research Organization (Chiba, Japan) which is in partnership with the National Disease Research Interchange (NDRI, Philadelphia, PA), and those from 10 donors were obtained from autopsy materials that were discarded after pathological investigation [14]. The use of the human livers was approved by the Ethics Committees of Kanazawa University (Kanazawa, Japan) and Iwate Medical University (Morioka, Japan). Microsomes fractions were prepared from 25 human livers according to the method described previously [15]. The protein concentration was determined using Bradford protein assay reagent (Bio-Rad, Hercules, CA) with γ-globulin as a standard. Total RNA was prepared using RNAiso and the integrity of the RNA was assessed by estimating the ratio of the band density of 28S and 18S rRNA.

2.8. SDS-PAGE and Western blot analyses of CYP2E1

Cell homogenates from HEK293/2E1 + UTR cells or HEK293/2E1 cells (10–40 μg) and human liver microsomes (3 μg) were separated on 10% SDS-PAGE and transferred to Immobilon-P transfer membrane (Millipore, Billerica, MA). The membrane was probed with goat anti-human CYP2E1 antibody. Biotinylated anti-goat IgG and a Vectastain ABC kit (Vector Laboratories, Burlingame, CA) were used for diaminobenzidine staining. As for cell homogenates from the HEK293 expression systems, the CYP2E1 protein level was normalized with the GAPDH protein level. As for human liver microsomes, a standard curve using recombinant human CYP2E1 expressed in baculovirus-infected insect cells (BD Gentest, Worburn, MA) was used to determine the absolute expression level of CYP2E1 protein. The quantitative analysis was performed using ImageQuant TL Image Analysis software (GE Healthcare Bio-Sciences).

2.9. Enzyme activity

Chlorzoxazone 6-hydroxylase activity was determined as follows: a typical incubation mixture (final volume of 0.2 ml) contained 50 mM potassium phosphate buffer (pH 7.4), 500 μM chlorzoxazone, and 0.5 mg/ml cell homogenates from HEK293/2E1 + UTR cells or HEK293/2E1 cells or human liver microsomes. The reaction was initiated by the addition of the NADPH-generating system (0.5 mM $NADP^+$, 5 mM glucose-6-phosphate, 5 mM $MgCl_2$, and 1 U/ml glucose-6-phosphate dehydrogenase) after 2 min preincubation at 37 °C. After the 10–30 min incubation at 37 °C, the reaction was terminated by the addition of 10 μl of ice-cold 10% perchloric acid. Coumarin (0.25–1 nmol) was added as an internal standard. After removal of the protein by centrifugation at 10,000 rpm for 5 min, a portion of the supernatant was subjected to high-performance liquid chromatography

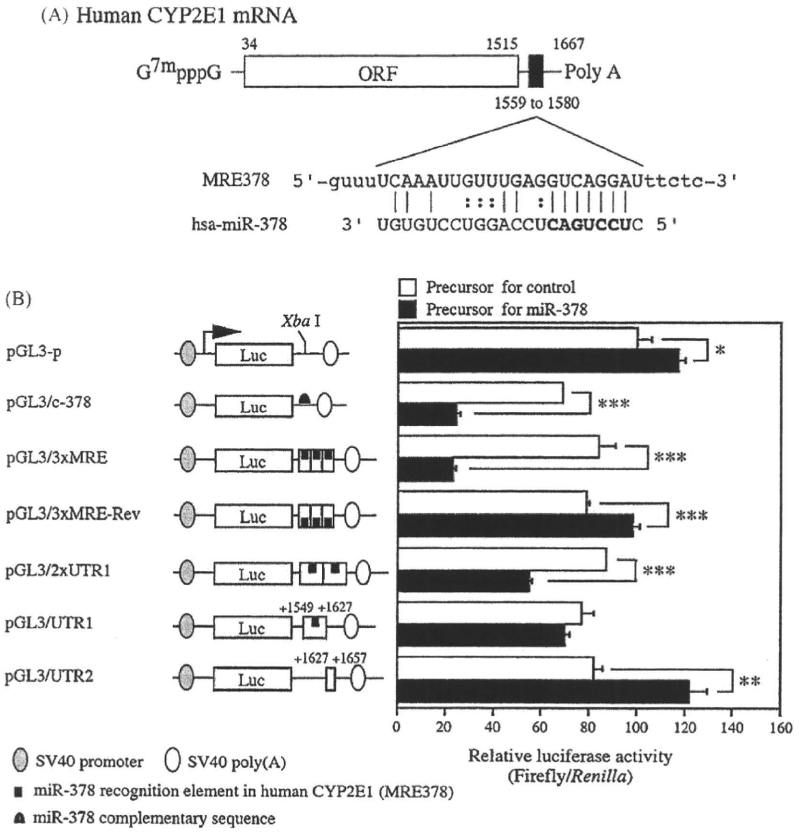

Fig. 1. Luciferase assay using the plasmids containing the MRE378 in the 3′-UTR of human CYP2E1 mRNA. Schematic representation of human CYP2E1 mRNA and the predicted target sequence of miR-378 (A). The numbering refers to the 5′ end of mRNA as 1, and the coding region is from +34 to +1515. MRE378 (from +1559 to +1580) is located on the 3′-UTR of human CYP2E1 mRNA. *bold letters*, seed sequence. Luciferase assays using the reporter plasmids containing various fragments downstream of the firefly luciferase gene (B). The reporter plasmids (170 ng) were transiently transfected with phRL-TK plasmid (30 ng) and 20 nM precursors for miR-378 or negative control #1 (control) into HEK293 cells. The firefly luciferase activity for each construct was normalized with the *Renilla* luciferase activities. Values are expressed as percentages of the relative luciferase activity of pGL3-p plasmid. Each column represents the mean ± SD of three independent experiments. $^*P < 0.05$, $^{**}P < 0.01$, $^{***}P < 0.001$, compared with the precursor for control.

(HPLC). The HPLC analyses were performed using an L-7100 pump (Hitachi, Tokyo, Japan), an L-7200 autosampler (Hitachi), an L-7405 UV detector (Hitachi), and a D-2500 chromato-integrator (Hitachi) equipped with a Mightysil RP-18 C18 GP (4.6 mm × 150 mm, 5 μm) column (Kanto Chemical, Tokyo, Japan). The eluent was monitored at 295 nm with a noise-base clean Uni-3 (Union, Gunma, Japan). The mobile phase was 28% methanol containing 50 mM potassium phosphate (pH 4.2). The flow rate was 1.0 ml/min. The column temperature was 35 °C. The quantification of the metabolites was performed by comparing the HPLC peak height with that of authentic standards with reference to an internal standard.

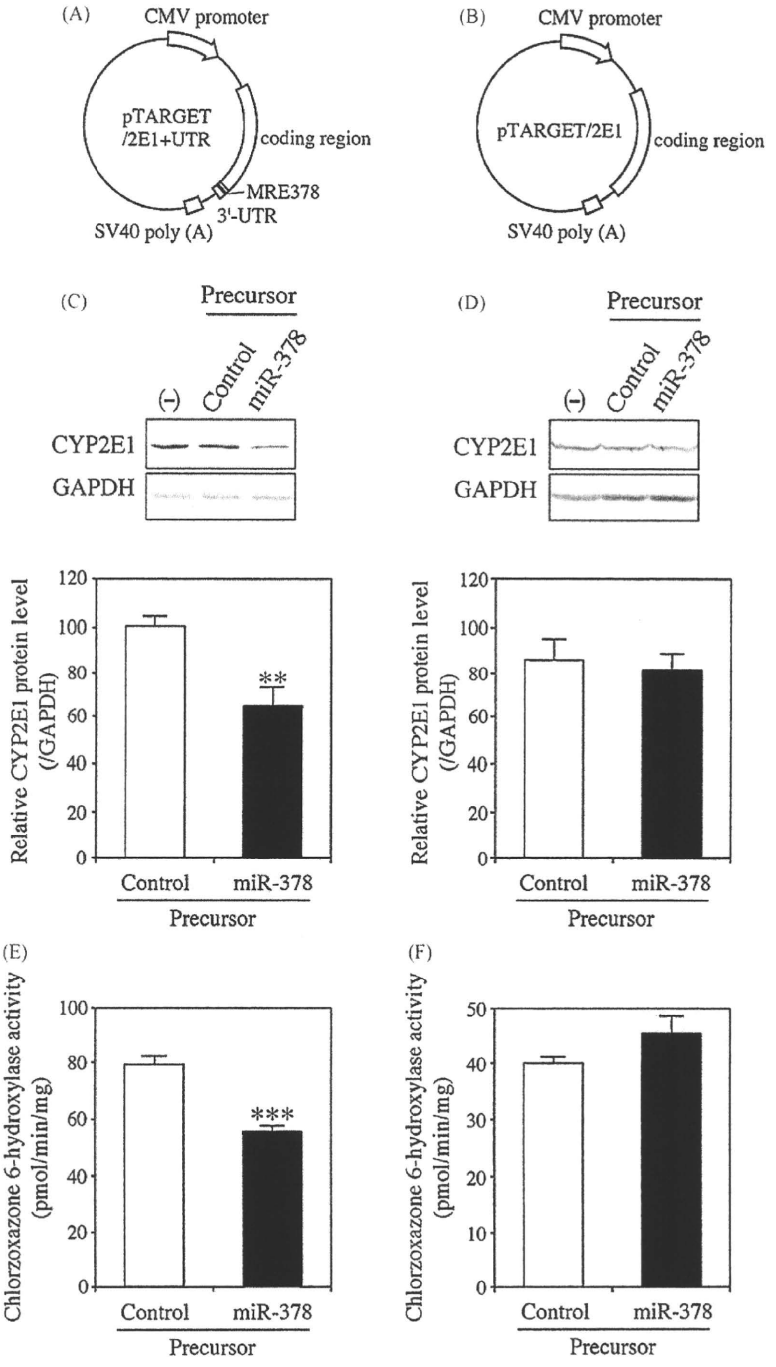

Fig. 2. Effects of overexpression of miR-378 on protein level and enzyme activity of CYP2E1. Schematic representation of the CYP2E1 expression plasmids including (A) or excluding (B) 3′-UTR of CYP2E1 (pTARGET/2E1-UTR or pTARGET/2E1). The CYP2E1 protein levels in HEK293/2E1 + UTR (C) and HEK293/2E1 (D) cells 48 h after the transfection of 10 nM precursors for miR-378 or negative control #1 (control). The CYP2E1 protein levels were determined by Western blot analysis and were normalized with the GAPDH protein level. Values are expressed as percentages relative to no transfection (−). Each column represents the mean ± SD of three independent experiments. $^{**}P < 0.01$, compared with the precursor for control. Enzyme activity of CYP2E1 in HEK293/2E1 + UTR (E) and HEK293/2E1 (F) cells 48 h after the transfection of 10 nM precursors for miR-378 or control. Chlorzoxazone 6-hydroxylase activity was measured using the cell homogenate at a substrate concentration of 500 μM. The control activities in homogenates from non-treated HEK293/2E1 + UTR (E) and HEK293/2E1 (F) cells were 70.5 ± 8.5 and 41.9 ± 1.0 pmol/min/mg, respectively. Each column represents the mean ± SD of three independent experiments. $^{***}P < 0.001$, compared with the precursor for control.

2.10. Real-time RT-PCR for CYP2E1

The cDNA was synthesized from total RNA using ReverTra Ace. The CYP2E1 mRNA levels were quantified by real-time RT-PCR using the Mx3000P™ (Stratagene). The forward and reverse primers for CYP2E1 mRNA were 5′-ACG GTA TCA CCG TGA CTG TGG-3′ and 5′-GCA TCT CTT GCC TAT CCT TGA-3′, respectively. A 1 μl portion of the reverse-transcribed mixture was added to a PCR mixture containing 10 pmol of each primer, 12.5 μl of SYBR Premix Ex Taq solution and 75 nM ROX in a final volume of 25 μl. The PCR condition was as follows: after an initial denaturation at 95 °C for 30 s, the amplification was performed by denaturation at 94 °C for 4 s, annealing and extension at 58 °C for 20 s for 45 cycles. The PCR product was digested with appropriate restriction enzymes to confirm that the amplicon was indeed CYP2E1. The CYP2E1 mRNA levels were normalized with GAPDH mRNA as described previously [16].

2.11. Real-time RT-PCR for mature miR-378

The expression levels of mature miR-378 in human livers were determined by TaqMan quantitative real-time PCR using the TaqMan microRNA assay (Applied Biosystems, Foster City, CA). The cDNA templates were prepared with the TaqMan microRNA Reverse Transcription kit which utilized the stem-loop reverse primers according to the manufacturer's protocols. After the reverse transcription reaction, the product was mixed with TaqMan Universal PCR Master Mix and TaqMan MicroRNA assay containing the forward and reverse primers as well as the TaqMan probe for miR-378. The PCR condition was as follows: after an initial denaturation at 95 °C for 10 min, the amplification was performed by denaturation at 95 °C for 15 s, annealing and extension at 60 °C for 60 s for 40 cycles. The expression levels of U6 small nuclear RNA (U6 snRNA) were also determined by TaqMan quantitative real-time PCR and were used to normalize the miR-378 levels.

2.12. Statistical analyses

Statistical significance was determined by unpaired, two-tailed student's *t*-test. Correlation analyses were performed by Pearson's product-moment method. A value of $P < 0.05$ was considered statistically significant.

3. Results

3.1. A miR-378 complementary sequence on the 3′-UTR of human CYP2E1 mRNA

The length of the 3′-UTR of human CYP2E1 is 152 bp. Computational prediction using miRBase Target database (http://microrna.sanger.ac.uk/) [17] indicated that 24 miRNAs including miR-378, miR-607, miR-223, and miR-105 share complementarity with sequences in the 3′-UTR. Meanwhile, when a Targetscan (http://www.targetscan.org/) was used, 6 miRNAs were found to share complementarity. The common miRNAs predicted in both web sites were only miR-378 and miR-607. We focused on miR-378 because it showed higher complementarity with the CYP2E1 mRNA (score 18.31 and energy −16.95) than the others. Fig. 1A shows the alignment of hsa-miR-378 with 3′-UTR of human CYP2E1 mRNA drawn using RNAhybrid (http://bibiserv.techfak.uni-bielefeld.de/rnahybrid/) [18]. We termed the sequence from +1559 to +1580 of the human CYP2E1 mRNA miR-378 recognition element (MRE378). We investigated whether the miR-378 might be involved in the regulation of CYP2E1 via the MRE378.

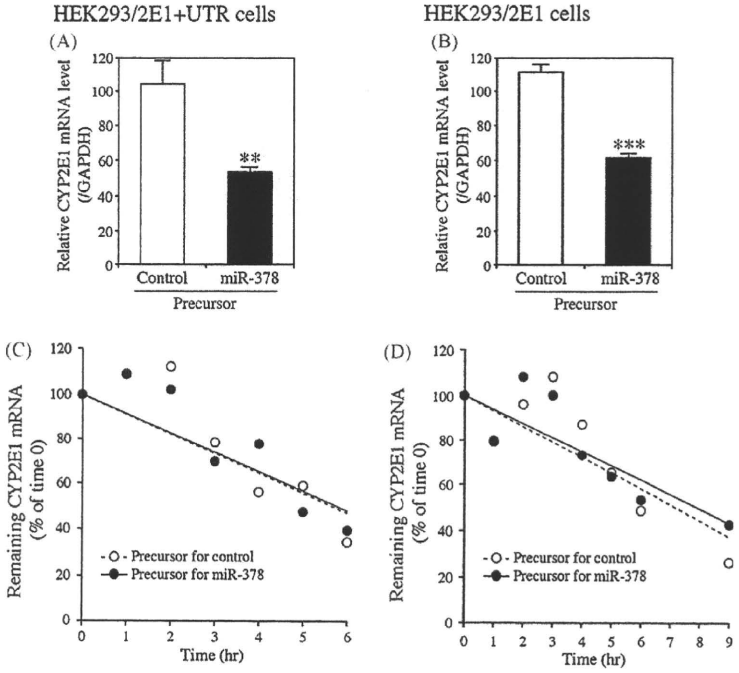

Fig. 3. Effects of overexpression of miR-378 on the CYP2E1 mRNA level and its stability. The CYP2E1 mRNA levels in HEK293/2E1 + UTR (A) and HEK293/2E1 (B) cells 48 h after the transfection of 10 nM precursors for miR-378 or negative control #1 (control). The CYP2E1 mRNA levels were determined by real-time RT-PCR and normalized with GAPDH mRNA. Values are expressed as percentages relative to no transfection. Each column represents the mean ± SD of three independent experiments. $^{**}P < 0.01$, $^{***}P < 0.001$, compared with the precursor for control. Stability of the CYP2E1 mRNA in the HEK293/2E1 + UTR (C) and HEK293/2E1 (D) cells. The cells transfected with 10 nM precursors for miR-378 or negative control #1 (control) were simultaneously treated with 2 μg/ml α-amanitin. Total RNA was prepared at 1, 2, 3, 4, 5, 6 and 9 h later. The CYP2E1 mRNA levels were determined by real-time RT-PCR and normalized with GAPDH mRNA. The amounts of mRNA at time 0 (the time of addition of α-amanitin) in each group (miR-378 or control treated) were assigned a value of 100%, and all other values at different time points were expressed as percentages of the time 0 value. Data are the mean of two independent experiments.

3.2. Luciferase assay to investigate whether the MRE378 is functional

To investigate whether MRE378 is functional in the regulation by miR-378, luciferase assays were performed using HEK293 cells (Fig. 1B) that barely express miR-378 (data not shown). We first confirmed that the luciferase activity of the pGL3/c-378 plasmid, which contains the miR-378 complementary sequence, was significantly ($P < 0.001$) decreased (35% of control) by the co-transfection of the precursor for miR-378. The luciferase activity of the pGL3/3xMRE plasmid containing three copies of the MRE378 was significantly ($P < 0.001$) decreased (27% of control) by the overexpression of miR-378, whereas that of the pGL3/3xMRE-Rev plasmid with the inverted MRE378 was not. The luciferase activity of pGL3/UTR1 plasmid containing the single insertion of MRE378 was decreased by the overexpression of miR-378 (91% of control), although the difference was statistically insignificant. The luciferase activity of the pGL3/2xUTR1 plasmid containing the double insertion of the MRE378 was significantly ($P < 0.001$) decreased (63% of control) by the overexpression of miR-378. In contrast, the luciferase activity of the pGL3/UTR2 plasmid containing the 3′-UTR sequence excluding MRE378 was increased by the overexpression of miR-378, although the reason is not clear. The luciferase activity of the pGL3-p plasmid was also increased by the overexpression of miR-378. Possibly, miR-378 might affect some factors for the SV40 promoter. This may suggest that the repressive effects of miR-378 on 3′-UTR of the reporter gene were underestimated. The results presented here suggest that miR-378 functionally recognized the MRE378 on the human CYP2E1 mRNA.

3.3. Effects of overexpression of miR-378 on protein level and enzyme activity of CYP2E1

Since the CYP2E1 expression levels in cell lines derived from human cancers are too low to be detected by Western blot analysis, we sought to establish cell lines expressing CYP2E1. To examine the role of MRE378 on the 3′-UTR of CYP2E1 gene, two HEK293 transfectants with pTARGET/CYP2E1 + UTR (Fig. 2A) and pTARGET/CYP2E1 (Fig. 2B) plasmids were established. When the miR-378 was overexpressed in HEK293/2E1 + UTR cells, the CYP2E1 protein level was significantly ($P < 0.01$) decreased (60% of control) (Fig. 2C). The chlorzoxazone 6-hydroxylase activity was also significantly ($P < 0.01$) decreased (70% of control) by the overexpression of miR-378 (Fig. 2E). In contrast, the overexpression of miR-378 did not affect the CYP2E1 protein level (Fig. 2D) and enzyme activity (Fig. 2F) in the HEK293/2E1 cells. These results clearly indicated that 3′-UTR including MRE378 plays an important role in the miR-378-dependent down-regulation of CYP2E1. In silico searches raised other candidates including miR-223 (score 17.51, energy −16.47) and miR-105 (score 16.97, energy −15.39) for human CYP2E1. However, the co-transfection of precursor for miR-223 or miR-105 into the HEK293/2E1 + UTR cells did not cause a decrease of the CYP2E1 protein (data not shown). Thus, we found that human CYP2E1 is specifically regulated by miR-378.

3.4. Effects of overexpression of miR-378 on the CYP2E1 mRNA level and its degradation

To investigate if the down-regulation of CYP2E1 by miR-378 involves mRNA degradation, we determined the CYP2E1 mRNA

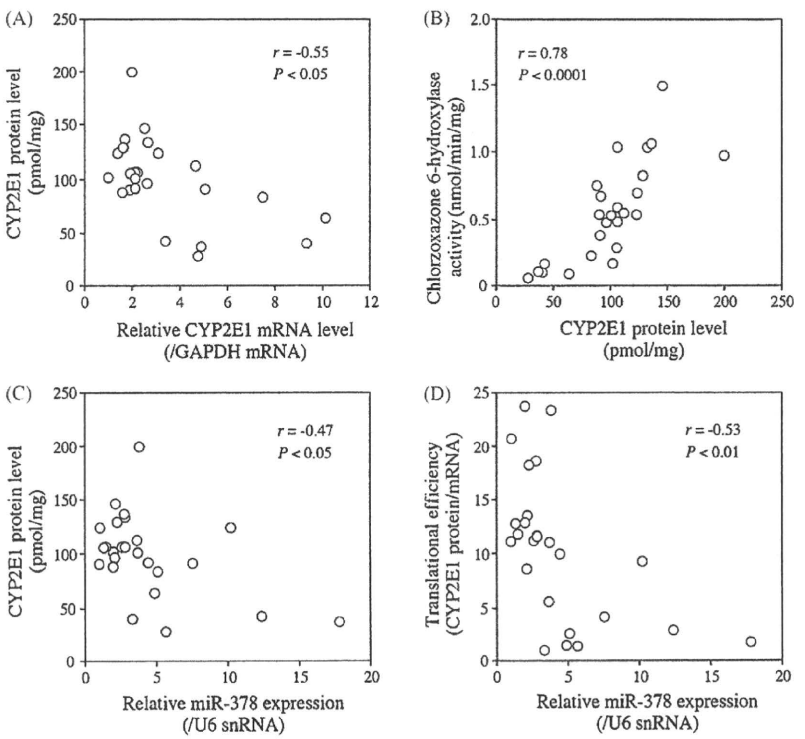

Fig. 4. Relationship between the miR-378, CYP2E1 mRNA, and CYP2E1 protein levels and enzyme activity in human livers. Relationship between the CYP2E1 mRNA and protein levels (A), the CYP2E1 protein levels and chlorzoxazone 6-hydroxylase activities (B), the miR-378 and CYP2E1 protein levels (C), and the miR-378 levels and translational efficiency of CYP2E1 (CYP2E1 protein/mRNA ratio) (D). The expression levels of miR-378 and CYP2E1 mRNA in a panel of 25 human livers were determined by real-time RT-PCR and normalized with U6 snRNA levels and GAPDH mRNA levels, respectively. The values represent the levels relative to that of the lowest sample. The absolute CYP2E1 protein levels were determined by Western blot analysis using a standard curve with recombinant human CYP2E1 protein. The chlorzoxazone 6-hydroxylase activity was measured using human liver microsomes at a substrate concentration of 500 μM. Data are the mean of two independent experiments.

levels. When the miR-378 was overexpressed in HEK293/2E1 + UTR cells, the CYP2E1 mRNA level was significantly ($P < 0.01$) decreased (51% of control) (Fig. 3A). Similarly, the CYP2E1 mRNA level was also significantly ($P < 0.001$) decreased (55% of control) in HEK293/2E1 cells (Fig. 3B). Next, we investigated whether miR-378 affects the stability of the CYP2E1 mRNA. When the HEK293/2E1 + UTR cells were treated with α-amanitin, an inhibitor of transcription, the half-life of the CYP2E1 mRNA was estimated to be 5.6 h (Fig. 3C). The overexpression of miR-378 did not affect the half-life. The half-life of the CYP2E1 mRNA in the HEK293/2E1 cells was 7.1 h (Fig. 3D), and it was not affected by the overexpression of miR-378. These results suggest that miR-378 did not affect the degradation of CYP2E1 mRNA.

3.5. Relationship between the expression levels of miR-378, CYP2E1 mRNA, and CYP2E1 protein in human livers

To investigate the impact of the miR-378 on the CYP2E1 regulation in human livers, we examined the relationship between the expression levels of miR-378, CYP2E1 mRNA and protein as well as enzyme activity using a panel of 25 human livers. The CYP2E1 mRNA levels showed 10-fold interindividual variability. The CYP2E1 protein levels (27.7–199.7 pmol/mg, 7-fold variability) were significantly ($r = 0.78$, $P < 0.0001$) correlated with the chlorzoxazone 6-hydroxylase activities (0.05–1.49 nmol/min/mg, 30-fold variability) (Fig. 4B), but were inversely correlated with the CYP2E1 mRNA levels ($r = -0.55$, $P < 0.05$) (Fig. 4A), supporting the involvement of post-transcriptional regulation. Interestingly, the miR-378 levels (18-fold variability) showed a significant inverse correlation with the CYP2E1 protein levels ($r = -0.47$, $P < 0.05$) (Fig. 4C) and the translational efficiency of CYP2E1 (CYP2E1 protein/mRNA ratio) ($r = -0.53$, $P < 0.01$) (Fig. 4D). These results suggest that miR-378-dependent regulation has a great impact on the CYP2E1 expression in human livers.

4. Discussion

Earlier studies have reported that the induction of CYP2E1 seems to be regulated at the post-transcriptional or post-translational levels by the stabilization of mRNA [4] or protection against the rapid degradation of protein [5,19]. To obtain a clue towards understanding the mechanisms, we investigated the possibility that miRNAs may be involved in the regulation of human CYP2E1. As the results, we found that the miR-378 is involved in the post-transcriptional regulation of CYP2E1.

The overexpression of miR-378 significantly decreased the CYP2E1 protein level and enzyme activity in the cells expressing CYP2E1 including 3′-UTR, but not in the cells expressing CYP2E1 excluding 3′-UTR indicating that the 3′-UTR plays a role in the miR-378-dependent repression. Unexpectedly, the CYP2E1 mRNA levels in both cell lines were decreased by the overexpression of miR-378. However, the miR-378 did not facilitate the degradation of the CYP2E1 mRNA. Therefore, the down-regulation of CYP2E1 by miR-378 would mainly be due to the translational repression, not the mRNA degradation. The decrease of the CYP2E1 mRNA levels in the absence of α-amanitin (Fig. 3A and B) suggests the possibility that miR-378 affects the transcription of CYP2E1. To examine the possibility that the miR-378 might affect the CMV promoter activity, we utilized other heterologous expression systems with the pTARGET vector (i.e., HEK/CYP2A6, HEK/UGT1A3, and HEK/UGT1A4). These heterologously expressed mRNA levels were not affected by the overexpression of miR-378 (data not shown). Therefore, it was concluded that the decrease of CYP2E1 mRNA level by miR-378 was not due to the effects on the CMV promoter. Although the cause of the decrease of CYP2E1 mRNA by miR-378 remains to be clarified, a major mechanism of the down-regulation of CYP2E1 by miR-378 would be the translational repression, supported by the inverse correlation between the miR-378 levels and translational efficiency of CYP2E1 (Fig. 4C).

The sequences of mature miR-378 are completely conserved among human, rat, and mouse, but the sequence of the 3′-UTR of CYP2E1 is poorly conserved. Therefore, the regulation of CYP2E1 by miR-378 would be specific in human. Further study is needed to determine whether other miRNAs except miR-378 might be involved in the regulation of the CYP2E1 in other species.

As for miR-378, it has been reported that it promotes cell survival, tumor growth, and angiogenesis by repressing the expression of Sufu (suppressor of fused) and Fus-1, which are tumor suppressors [20]. Hua et al. [21] have reported that miR-378 binds to the 3′-UTR of vascular endothelial growth factor (VEGF) competing with other miRNAs and promotes the expression of VEGF. In addition to these studies, we provide new information concerning the role of miR-378 from pharmacological and toxicological aspects.

The gene coding miR-378 is within the intron 1 of the *peroxisome-proliferator-activated receptor-γ co-activator 1β (PGC1β)* gene on human chromosome 5q33.1 (http://microrna.sanger.ac.uk/sequences/). This means that the expression of miR-378 would be in parallel with that of PGC1β. PGC1β is known as a regulator of hepatic lipid synthesis and lipoprotein production [22]. It has been reported that the expression of PGC1β is down-regulated in diabetes or obesity, but up-regulated by insulin treatment [23,24]. In contrast, the expression of CYP2E1 is up-regulated in diabetes or obesity, but down-regulated by insulin treatment [25–27]. It would be of interest to investigate the expression of miR-378 in these pathophysiological conditions with reference to the changes in the CYP2E1 expression. In addition, the changes in the expression of miR-378 under the treatment with typical chemical inducers of CYP2E1 *in vivo* or *in vitro* are worth pursuing in the future.

In conclusion, we found that human CYP2E1 expression is regulated by miR-378, mainly via translational repression. This study should provide new insight into the unsolved mechanism of the post-transcriptional regulation of CYP2E1.

Acknowledgements

This work was supported in part by Grant-in-Aid for Scientific Research (B) from Japan Society for the Promotion of Science. We acknowledge Mr. Brent Bell for reviewing the manuscript.

References

[1] Lu Y, Cederbaum AI. CYP2E1 and oxidative liver injury by alcohol. Free Radic Biol Med 2008;44:723–38.
[2] Bolt HM, Roos PH, Thier R. The cytochrome P-450 isoenzyme CYP2E1 in the biological processing of industrial chemicals: consequences for occupational and environmental medicine. Int Arch Occup Environ Health 2003;76:174–85.
[3] Song BJ, Gelboin HV, Park SS, Yang CS, Gonzalez FJ. Complementary DNA and protein sequences of ethanol-inducible rat and human cytochrome P-450s. Transcriptional and post-transcriptional regulation of the rat enzyme. J Biol Chem 1986;261:16689–97.
[4] Song BJ, Matsunaga T, Hardwick JP, Park SS, Veech RL, Yang CS, et al. Stabilization of cytochrome P450j messenger ribonucleic acid in the diabetic rat. Mol Endocrinol 1987;1:542–7.
[5] Roberts BJ, Song BJ, Soh Y, Park SS, Shoaf SE. Ethanol induces CYP2E1 by protein stabilization. Role of ubiquitin conjugation in the rapid degradation of CYP2E1. J Biol Chem 1995;270:29632–5.
[6] Sumida A, Kinoshita K, Fukuda T, Matsuda H, Yamamoto I, Inaba T, et al. Relationship between mRNA levels quantified by reverse transcription-competitive PCR and metabolic activity of CYP3A4 and CYP2E1 in human liver. Biochem Biophys Res Commun 1999;262:499–503.
[7] Bièche I, Narjoz C, Asselah T, Vacher S, Marcellin P, Lidereau R, et al. Reverse transcriptase-PCR quantification of mRNA levels from cytochrome (CYP)1, CYP2 and CYP3 families in 22 different human tissues. Pharmacogenet Genomics 2007;17:731–42.
[8] Shimada T, Yamazaki H, Mimura M, Inui Y, Guengerich FP. Interindividual variations in human liver cytochrome P-450 enzymes involved in the oxida-

tion of drugs, carcinogens and toxic chemicals: studies with liver microsomes of 30 Japanese and 30 Caucasians. J Pharmacol Exp Ther 1994;270:414–23.
[9] Bartel DP. MicroRNAs: genomics, biogenesis, mechanism, and function. Cell 2004;116:281–97.
[10] Ambros V. The functions of animal microRNAs. Nature 2004;431:350–5.
[11] Calin GA, Sevignani C, Dumitru CD, Hyslop T, Noch E, Yendamuri S, et al. Human microRNA genes are frequently located at fragile sites and genomic regions involved in cancers. Proc Natl Acad Sci USA 2004;101:2999–3004.
[12] Lu J, Getz G, Miska EA, Alvarez-Saavedra E, Lamb J, Peck D, et al. MicroRNA expression profiles classify human cancers. Nature 2005;435:834–8.
[13] Lewis BP, Burge CB, Bartel DP. Conserved seed pairing, often flanked by adenosines, indicates that thousands of human genes are microRNA targets. Cell 2005;120:15–20.
[14] Izukawa T, Nakajima M, Fujiwara R, Yamanaka H, Fukami T, Takamiya M, et al. Quantitative analysis of UDP-glucuronosyltransferase (UGT) 1A and UGT2B expression levels in human livers. Drug Metab Dispos 2009;37:1759–68.
[15] Tabata T, Katoh M, Tokudome S, Hosokawa M, Chiba K, Nakajima M, et al. Bioactivation of capecitabine in human liver: involvement of the cytosolic enzyme on 5′-deoxy-5-fluorocytidine formation. Drug Metab Dispos 2004;32:762–7.
[16] Tsuchiya Y, Nakajima M, Kyo S, Kanaya T, Inoue M, Yokoi T. Human CYP1B1 is regulated by estradiol via estrogen receptor. Cancer Res 2004;64:3119–25.
[17] Griffiths-Jones S. The microRNA registry. Nucleic Acids Res 2004;32:D109–11.
[18] Rehmsmeier M, Steffen P, Hochsmann M, Giegerich R. Fast and effective prediction of microRNA/target duplexes. RNA 2004;10:1507–17.
[19] Song BJ, Veech RL, Park SS, Gelboin HV, Gonzalez FJ. Induction of rat hepatic *N*-nitrosodimethylamine demethylase by acetone is due to protein stabilization. J Biol Chem 1989;264:3568–72.
[20] Lee DY, Deng Z, Wang CH, Yang BB. MicroRNA-378 promotes cell survival, tumor growth, and angiogenesis by targeting SuFu and Fus-1 expression. Proc Natl Acad Sci USA 2007;104:20350–5.
[21] Hua Z, Lv Q, Ye W, Wong CK, Cai G, Gu D, et al. MiRNA-directed regulation of VEGF and other angiogenic factors under hypoxia. PLoS ONE 2006;1:e116.
[22] Lin J, Yang R, Tarr PT, Wu PH, Handschin C, Li S, et al. Hyperlipidemic effects of dietary saturated fats mediated through PGC-1β coactivation of SREBP. Cell 2005;120:261–73.
[23] Crunkhorn S, Dearie F, Mantzoros C, Gami H, da Silva WS, Espinoza D, et al. Peroxisome proliferator activator receptor γ coactivator-1 expression is reduced in obesity: potential pathogenic role of saturated fatty acids and p38 mitogen-activated protein kinase activation. J Biol Chem 2007;282:15439–50.
[24] Liu HY, Yehuda-Shnaidman E, Hong T, Han J, Pi J, Liu Z, et al. Prolonged exposure to insulin suppresses mitochondrial production in primary hepatocytes. J Biol Chem 2009;284:14087–95.
[25] Wang Z, Hall SD, Maya JF, Li L, Asghar A, Gorski JC. Diabetes mellitus increases the in vivo activity of cytochrome P450 2E1 in humans. Br J Clin Pharmacol 2003;55:77–85.
[26] De Waziers I, Garlatti M, Bouguet J, Beaune PH, Barouki R. Insulin down-regulates cytochrome P450 2B and 2E expression at the post-transcriptional level in the rat hepatoma cell line. Mol Pharmacol 1995;47:474–9.
[27] Woodcroft KJ, Hafner MS, Novak RF. Insulin signaling in the transcriptional and posttranscriptional regulation of CYP2E1 expression. Hepatology 2002;35:263–73.

Toxicology 275 (2010) 50–57

Contents lists available at ScienceDirect

Toxicology

journal homepage: www.elsevier.com/locate/toxicol

Interleukin-17 is involved in α-naphthylisothiocyanate-induced liver injury in mice

Masanori Kobayashi[a], Satonori Higuchi[a], Katsuhiko Mizuno[a], Koichi Tsuneyama[b], Tatsuki Fukami[a], Miki Nakajima[a], Tsuyoshi Yokoi[a,*]

[a] Drug Metabolism and Toxicology, Faculty of Pharmaceutical Sciences, Kanazawa University, Kakuma-machi, Kanazawa 920-1192, Japan
[b] Department of Diagnostic Pathology, Graduate School of Medicine and Pharmaceutical Science for Research, University of Toyama, Sugitani, Toyama 930-0194, Japan

ARTICLE INFO

Article history:
Received 2 April 2010
Received in revised form 23 May 2010
Accepted 31 May 2010
Available online 8 June 2010

Keywords:
Drug-induced liver injury
Cytokines
MIP-2
Neutrophils
Helper T cells

ABSTRACT

Drug-induced liver injury (DILI) is a major safety concern in drug development and clinical drug therapy. The pathogenesis of DILI usually involves the participation of the parent drug or metabolites that either directly affect the cell biochemistry or elicit an immune response. However, in most cases the mechanisms are unknown. Alpha-naphthylisothiocyanate (ANIT) is known as a hepatotoxicant that causes biliary cell and hepatocyte damage and induces intense neutrophil infiltration in the liver. To investigate whether an immune-mediated mechanism is involved in ANIT-induced liver injury, we examined the plasma AST, ALT and T-Bil levels, hepatic expression of transcriptional factors, cytokines and CXC chemokine genes, plasma IL-17 level and histopathological changes in liver after ANIT administration in mice. Hepatic mRNA expression of retinoid related orphan receptor γt (RORγt) and macrophage inflammatory protein (MIP-2) and plasma IL-17 level was significantly increased in ANIT-administered mice as well as the plasma AST, ALT and T-Bil. Neutralization of IL-17 using anti-IL-17 antibody (100 μg/mouse, single i.p.) suppressed the hepatotoxic effect of ANIT. Co-administration of recombinant IL-17 (1 μg/mouse, single i.p.) to ANIT-administered mice resulted in a remarkable increase of the plasma AST, ALT and T-Bil levels. In conclusion, it was firstly demonstrated that IL-17 is involved in the ANIT-induced liver injury in mice.

1. Introduction

Drug-induced liver injury (DILI) is a major reason for the withdrawal of approved drugs from the market. Some drugs such as tienilic acid, amodiaquine and halothane induce hepatic hypersensitivity reactions (Bugelski, 2005). The pathogenesis of drug-induced liver injury usually involves the participation of the parent drug or metabolites that either directly affect the cell biochemistry or elicit an immune response. In most cases, the mechanisms of DILI are still unknown and predictive experimental animal models are lacking.

Helper T cells (Th cells) are an important regulator of acquired immunity. Th cells are subdivided into Th1, Th2, regulatory T cells (Treg) and Th17 by their unique production of cytokines and characteristic transcription factors (Kidd, 2003; Zhu and Paul, 2008). Th1 cells mediate immune responses against intracellular pathogens and play an important role in resistance to mycobacterial infections. Th2 cells mediate host defense against extracellular parasites and are important in the induction and persistence of asthma and other allergic disease. Treg cells play a critical role in maintaining self-tolerance as well as in regulating immune responses (Zhu and Paul, 2008). Th17 cells, which mainly produce IL-17, play critical roles in the protection against microbial challenges and the induction of autoimmune diseases, and IL-17 can induce many inflammatory cytokines and CXC chemokines (such as MIP-2 and keratinocyte-derived chemokine) resulting in neutrophil infiltration and activation (Zhu and Paul, 2008). One of the causes of DILI is thought to be related to immune-mediated reactions. We previously reported that IL-17 is involved in halothane-induced liver injury in mice (Kobayashi et al., 2009).

Alpha-naphthylisothiocyanate (ANIT) is known as a hepatotoxicant that causes hepatocyte and biliary cell damage and is used in rodents as a model of human intrahepatic cholestasis. ANIT is conjugated with glutathione (GSH) in hepatocytes (Carpenter-Deyo et al., 1991). The GSH–ANIT conjugate is transported by the canalicular efflux transporter, multidrug resistance-associated protein 2 (Mrp2) into bile, and there dissociates into free GSH and ANIT (Dietrich et al., 2001). The reuptake of ANIT in bile by hepatocytes leads to high concentrations of ANIT in the biliary cells. This repetitive round of secretion and reuptake contributes to the hepatotoxicity directly (Dietrich et al., 2001; Jean and Roth, 1995).

* Corresponding author. Tel.: +81 76 234 4407; fax: +81 76 234 4407.
E-mail address: tyokoi@kenroku.kanazawa-u.ac.jp (T. Yokoi).

0300-483X/$ – see front matter © 2010 Elsevier Ireland Ltd. All rights reserved.
doi:10.1016/j.tox.2010.05.011

Table 1
Sequences of primers and annealing temperatures used for real-time RT-PCR analyses.

Target	Primer	Sequence	Annealing temperature (°C)
T-bet	FP	5′-CAA GTG GGT GCA GTG TGG AAA G-3′	68
	RP	5′-TGG AGA GAC TGC AGG ACG ATC-3′	
GATA-3	FP	5′-GGA GGA CTT CCC CAA GAG CA-3′	68
	RP	5′-CAT GCT GGA AGG GTG GTG A-3′	
RORγt	FP	5′-ACC TCC ACT GCC AGC TGT GTG CTG TC-3′	68
	RP	5′-TCA TTT CTG CAC TTC TGC ATG TAG ACT GTC CC-3′	
FoxP3	FP	5′-CTA GCA GTC CAC TTC ACC AAG-3′	66
	RP	5′-GCT GCT GAG ATG TGA GTG TC-3′	
IFNγ	FP	5′-GGC CAT CAG CAA CAT AAG C-3′	68
	RP	5′-TGG ACC ACT CGG ATG AGC TCA-3′	
IL-10	FP	5′-TGA AGA CCC TCA GGA TGC GG-3′	66
	RP	5′-AGA GCT CTG TCT AGG TCC TGG-3′	
TNFα	FP	5′-TGT CTC AGC CTC TTC TCA TTC C-3′	66
	RP	5′-TGA GGG TCT GGG CCA TAG AAC-3′	
MIP-2	FP	5′-AAG TTT GCC TTG ACC CTG AAG-3′	64
	RP	5′-ATC AGG TAC GAT CCA GGC TTC-3′	
GAPDH	FP	5′-AAA TGG GGT GAG GCC GGT-3′	64
	RP	5′-ATT GCT GAC AAT CTT GAG TGA-3′	

FP, forward primer, RP, reverse primer.

Meanwhile, ANIT also is known to induce intense neutrophil infiltrations primarily in the periportal area of the liver (Dahm et al., 1991). Dahm et al. (1991) also demonstrated that depletion of circulating neutrophils attenuates ANIT-induced liver injury, emphasizing the importance of the inflammatory reaction in the liver injury.

In this study, we investigated whether Th cells are involved in ANIT-induced liver injury in mice. First, the hepatic expressions of T box expressed in T cells (T-bet), GATA-binding protein (GATA-3), forkhead box P3 (FoxP3) and retinoid related orphan receptor γt (RORγt), which are transcriptional factors for Th1, Th2, Treg and Th17 cells, respectively, and cytokines specific for helper T cells were measured after ANIT administration to mice. Secondly, to investigate the IL-17 involvement, the plasma IL-17 levels were measured, and neutralization and administration of recombinant IL-17 were performed.

2. Materials and methods

2.1. Chemicals

α-Naphthylisothiocyanate (ANIT) was purchased from Wako Pure Chemical Industries (Osaka, Japan). RNAiso was from Nippon Gene (Tokyo, Japan). Rever-Tra Ace was from Toyobo (Tokyo, Japan). Random hexamer and SYBR Premix Ex Taq were from Takara (Osaka, Japan). All primers were commercially synthesized at Hokkaido System Sciences (Sapporo, Japan). Monoclonal anti-mouse IL-17 antibody,

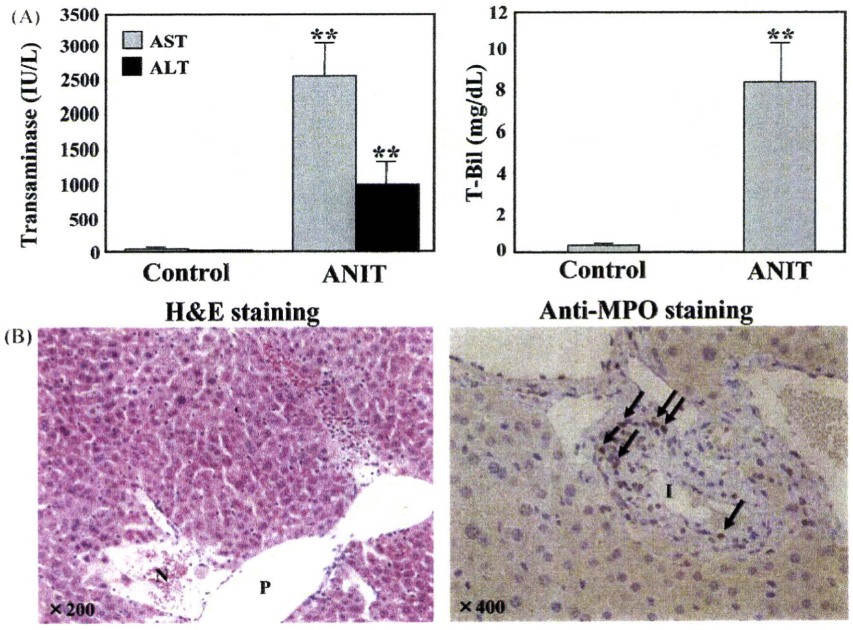

Fig. 1. Plasma AST, ALT and T-Bil levels and histopathological presentation of liver injury in ANIT-administered mice.
Mice were administered ANIT (50 mg/kg, p.o.), and plasma for AST and ALT (A) and T-Bil (B) was collected 24 h after administration. Data are mean ± SD of 6 mice. Significantly different from control group (**$P < 0.01$). Histopathological examination of the liver (C). Liver specimens were sampled 24 h after ANIT administration. The liver tissue sections were stained with H&E or immunostained with anti-MPO antibody. Arrows indicated MPO-positive cells. N, necrotic area; P, portal vein; I, intralobular bile duct.

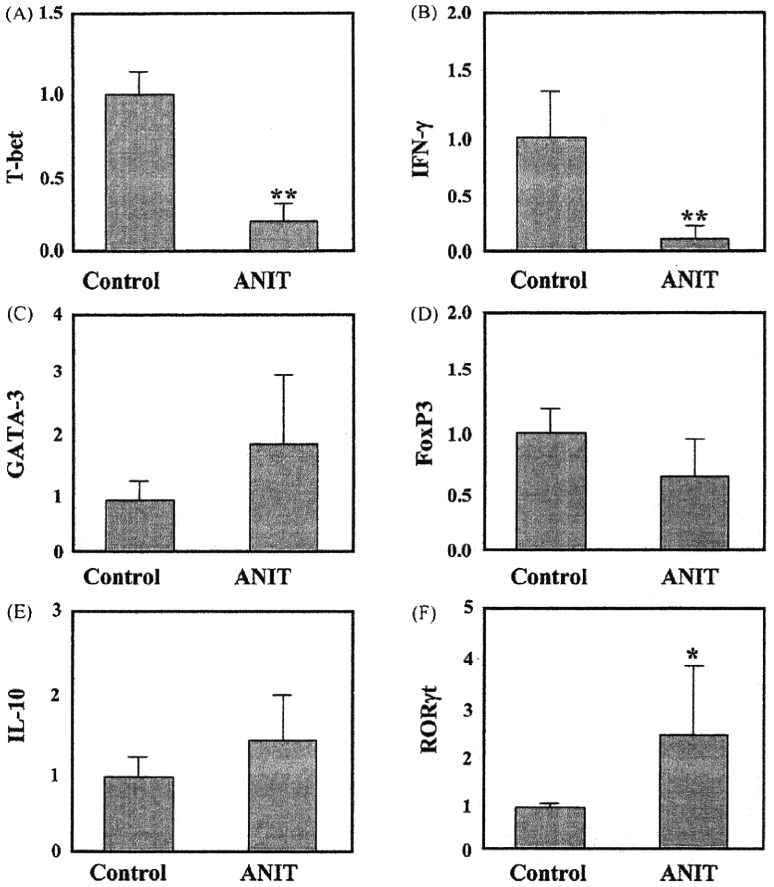

Fig. 2. Hepatic mRNA expression of transcriptional factors and cytokine genes 24 h after ANIT administration.
Relative expressions of T-bet (A), IFN-γ (B), GATA-3 (C), FoxP3 (D), IL-10 (E) and RORγt (F) were measured by real-time RT-PCR and normalized to GAPDH mRNA. Data are mean ± SD of 6 mice. Significantly different from control group ($^{*}P < 0.05$ and $^{**}P < 0.01$).

rat IgG2a isotype and recombinant mouse IL-17 were from R&D Systems (Abingdon, UK). A Ready-SET-GO! Mouse Interleukin-17A (IL-17A) enzyme-linked immunosorbent assay (ELISA) kit was from eBioscience (San Diego, CA). Dri-Chem 4000 was from FUJIFILM Corporation (Saitama, Japan). Other chemicals were of analytical or the highest grade commercially available.

2.2. ANIT-administration

Female BALB/cCrSlc mice (6 weeks old, 15–20 g) were obtained from SLC Japan (Hamamatsu, Japan). Animals were housed in a controlled environment (temperature 25 ± 1 °C, humidity 50 ± 10%, and 12-h light/12-h dark cycle) in the institutional animal facility with access to food and water *ad libitum*. Animals were acclimatized before use for the experiments. ANIT was dissolved in olive oil (10 mg/mL) and orally administered to mice at a dose of 50 mg/kg following overnight fasting. An hour after ANIT administration, mice were returned to access to food and water *ad libitum*. Twenty-four hours after ANIT administration, the animals were sacrificed and the blood and livers were collected. A portion of each excised liver was fixed in 10% formalin neutral buffer solution and used for immunohistochemical staining. The degree of liver injury was assessed by hematoxylin–eosin (H&E) staining, and the plasma aspartate aminotransferase (AST), alanine aminotransferase (ALT), and total bilirubin (T-Bil) levels were measured by Dri-Chem 4000 according to the manufacturer's instructions. The neutrophil infiltration was assessed by immunostaining for myeloperoxidase (MPO). Animal maintenance and treatment were conducted in accordance with the National Institutes of Health Guide for Animal Welfare of Japan, as approved by the Institutional Animal Care and Use Committee of Kanazawa University, Japan.

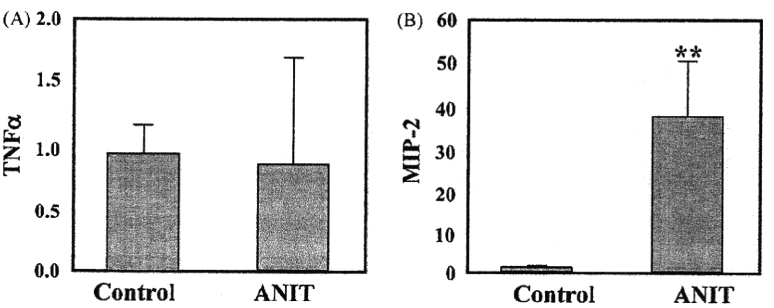

Fig. 3. Hepatic mRNA expression of proinflammatory cytokine and CXC chemokine.
Relative expressions of TNFα (A) and MIP-2 (B) were measured by real-time RT-PCR and normalized to GAPDH mRNA. Data are mean ± SD of 6 mice. Significantly different from control group ($^{**}P < 0.01$).

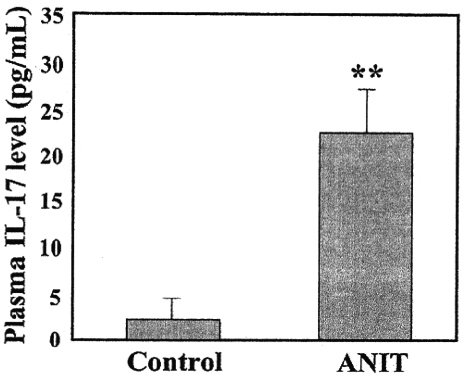

Fig. 4. Plasma IL-17 levels 24 h after ANIT administration.
The plasma IL-17 level was measured 24 h after ANIT administration to mice using ELISA. Data are mean ± SD of 6 mice. Significantly different from control group (**$P < 0.01$).

2.3. Real-time reverse transcription (RT)-PCR

RNA from the mouse liver was isolated using RNAiso according to the manufacturer's instructions. T-bet, GATA-3, RORγt, FoxP3, IFN-γ, IL-10, tumor necrosis factor α (TNFα), macrophage inflammatory ptrotein-2 (MIP-2) and GAPDH were quantified by real-time RT-PCR. The primer sequences used in this study are shown in Table 1. For the RT-process, total RNA (10 μg) and 150 ng random hexamer were mixed and incubated at 70 °C for 10 min. RNA solution was added to a reaction mixture containing 100 units of ReverTra Ace, reaction buffer and 0.5 mM dNTPs in a final volume of 40 μL. The reaction mixture was incubated at 30 °C for 10 min, 42 °C for 1 h, and heated at 98 °C for 10 min to inactivate the enzyme. The real-time RT-PCR was performed using the Mx3000P (Stratagene, La Jolla, CA). The PCR mixture contained 1 or 2 μL of template cDNA, SYBR Premix Ex Taq solution and 8 pmol of forward and reverse primers. Amplified products were monitored directly by measuring the increase of the dye intensity of the SYBR Green I (Molecular Probes, Eugene, OR) that binds to the double-strand DNA amplified by PCR.

2.4. Administration of anti-mouse IL-17 antibody or recombinant mouse IL-17

Nine hours after ANIT administration, mice were administered anti-mouse IL-17 antibody intraperitoneally (100 μg of anti-mouse IL-17 antibody in 0.5 mL of sterile PBS). As a control, rat IgG2a was administered (100 μg of rat IgG2a in 0.5 mL of sterile PBS). Recombinant mouse IL-17 was intraperitoneally administered (1 μg of recombinant IL-17 in 0.2 mL of sterile PBS containing 0.5% BSA) immediately after ANIT administration.

2.5. Measurement of plasma IL-17 level

The plasma IL-17 level was measured by enzyme-linked immunosorbent assay (ELISA) using a Ready-SET-GO! Mouse Interleukin-17A (IL-17A) kit from eBioscience according to the manufacturer's instructions.

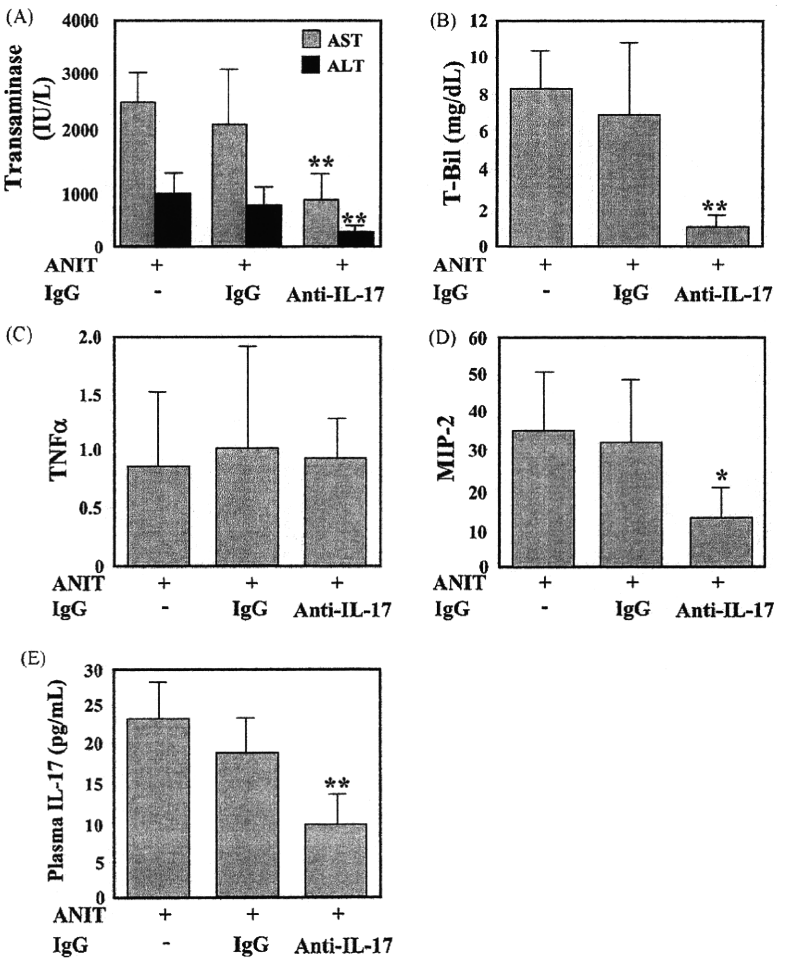

Fig. 5. Effect of anti-mouse IL-17 antibody on plasma AST, ALT and T-Bil, hepatic mRNA expression of TNFα and MIP-2 and plasma IL-17 levels in ANIT-administered mice. Mice were injected monoclonal anti-mouse IL-17 antibody (100 μg/mouse, i.p.) or rat IgG2a 9 h after the ANIT administration. Twenty-four hours after ANIT administration, plasma for the AST, ALT and T-Bil analyses was collected (A and B). Relative expressions of hepatic TNFα (C) and MIP-2 (D) mRNA were measured by real-time RT-PCR and normalized to GAPDH mRNA. The plasma IL-17 level was measured using ELISA (E). Data are mean ± SD of 5–6 mice. Significantly different from the ANIT-administered group (*$P < 0.05$ and **$P < 0.01$).

2.6. Quantitation of hepatic MPO-positive cells

Five visual fields of ×400 magnification (0.1 mm² each) were randomly selected from each MPO-immunostained specimen and taken picture by digital camera (D-33E, OLYMPUS, Tokyo). The MPO-positive mononuclear cells were counted from five pictures of each specimen. The total number of MPO-positive cells from five randomly selected visual fields was compared amongst the specimens.

2.7. Statistical analysis

Statistical analyses were performed with SAS 9.1.3. Comparison of two groups was made with Wilcoxon test. Comparison of multiple groups was made with non-parametrical Dunnet test using joint rankings. $P < 0.05$ was considered statistically significant.

3. Results

3.1. Increase of plasma AST, ALT and T-Bil levels in ANIT-administered mice

Female BALB/c mice were administered ANIT at a dose of 50 mg/kg. The dose of ANIT was determined as described by Kodali et al. (2006). A marked increase of the AST, ALT and T-Bil levels in plasma was observed 24 h after ANIT administration (Fig. 1A and B).

3.2. Histopathological changes in mouse liver after ANIT administration

Histopathological changes in mouse liver 24 h after ANIT administration are shown in Fig. 1C. In H&E staining, lack of hepatocytes due to necrosis and infiltration of inflammation cells such as neutrophils and mononuclear cells around the portal area was observed (Fig. 1C). In addition, the destruction and degeneration of the interlobular bile ducts occurred. Immunohistochemically, most of the infiltrating cells reacted to anti-MPO antibody 24 h after ANIT administration.

3.3. Expression of transcription factors and cytokine genes in ANIT-administered mouse liver

To investigate the involvement of Th cells in the ANIT-induced liver injury, the hepatic mRNA expression levels of transcriptional factors for each T helper lineage were measured by real-time RT-PCR (Fig. 2). The hepatic mRNA expression level of T-bet, which is a master regulator of Th1 cells, in ANIT-administered mice was significantly decreased to 16% compared with that of control mice (Fig. 2A). The hepatic mRNA expression level of interferon-γ (IFN-γ), which is a major cytokine of Th1 cells, significantly decreased after ANIT administration compared with that of control mice (Fig. 2B). Hepatic mRNA expression levels of GATA-3 and FoxP3 in ANIT-administered mice showed tendencies to increase and decrease, respectively (Fig. 2C and D). There was no difference in the hepatic mRNA expression level of IL-10 between ANIT-treated and control mice (Fig. 2D). Hepatic mRNA expression level of RORγt, which is master regulator for Th17 cells, was shown 2.5-fold higher in ANIT-administered than in control mice (Fig. 2E).

3.4. Changes of proinflammatory cytokine and CXC chemokine

To investigate whether the changes in liver injury and neutrophil infiltration observed in ANIT-administered mice resulted from the increases of proinflammatory cytokines and CXC chemokines, hepatic TNFα and MIP-2 mRNA expressions were measured. TNFα mRNA was not changed by ANIT administration (Fig. 3A). However, MIP-2 mRNA was markedly increased 24 h after ANIT administration (Fig. 3B).

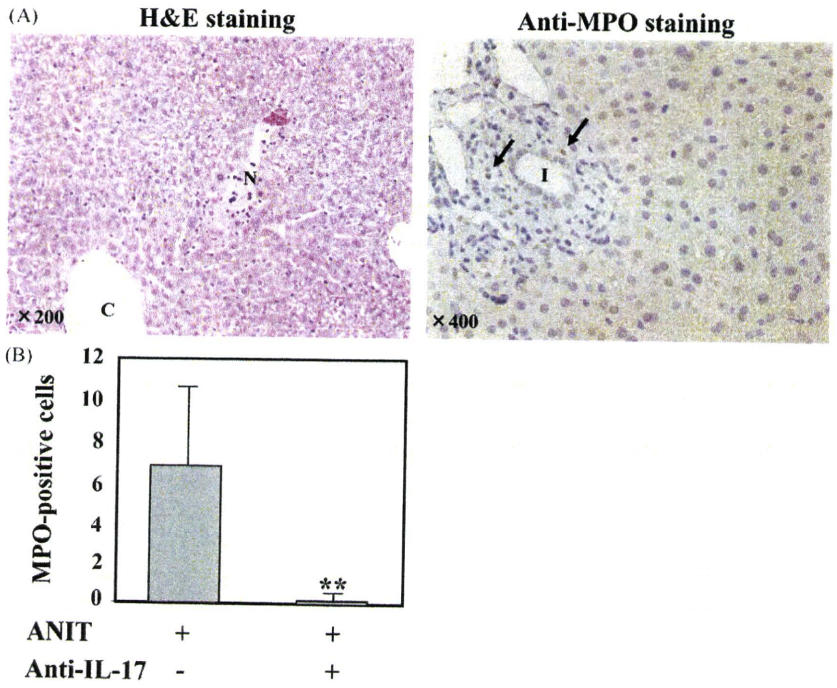

Fig. 6. Effect of anti-mouse IL-17 antibody on histopathological changes of liver injury in ANIT-administered mice and number of hepatic MPO-positive cells.
Mice were injected monoclonal anti-mouse IL-17 antibody (100 μg/mouse, i.p.) 9 h after the ANIT administration. Liver specimens were sampled 24 h after the ANIT administration. The liver tissue sections were stained with H&E or immunostained with anti-MPO antibody (A). Arrows indicated MPO-positive cells. C, central vein; N, necrotic area; I, intralobular bile duct.
The number of MPO-positive mononuclear cells was counted from five pictures of each specimen. The total number of MPO-positive cells from five randomly selected visual fields was compared with mice administered ANIT alone (B). Significantly different from ANIT-administered group (**$P < 0.01$).

3.5. Changes of plasma IL-17 levels

IL-17 plays an important role in neutrophil infiltration and activation. The hepatic mRNA expression level of RORγt, which is a master regulator for Th17 cells, was increased after ANIT administration. Then, the plasma IL-17 level was measured using ELISA. The plasma IL-17 level in ANIT-administered mice was significantly increased (9.5-fold) compared with control mice (Fig. 4).

3.6. Effects of anti-IL-17 antibody administration in ANIT-administered mice

To investigate whether IL-17 was involved in the ANIT-induced liver injury, we conducted a neutralization study. In the neutralization study, a monoclonal anti-mouse IL-17 antibody injected intraperitoneally 9 h after ANIT administration significantly reduced the plasma AST, ALT and T-Bil levels at 24 h after ANIT administration (Fig. 5A and B). There were no significant differences in the hepatic mRNA expressions of TNFα, however hepatic MIP-2 mRNA was significantly decreased compared with mice administered ANIT alone (Fig. 5C and D). The plasma IL-17 level in anti-mouse IL-17 antibody-treated mice was significantly decreased compared with mice administered ANIT alone (Fig. 5E). In the histopathological study, no lack of hepatocytes or destruction of the interlobular bile ducts around the portal area was observed, and the number of MPO positive cells was decreased in ANIT and anti-mouse IL-17 antibody-administered mice (Fig. 6A and B) compared with mice administered ANIT alone (Fig. 1C). These effects were not observed by the administration of rat IgG2a.

3.7. Recombinant IL-17 exacerbated hepatotoxic effect of ANIT

To further investigate whether IL-17 was involved in the ANIT-induced liver injury, we performed a recombinant mouse IL-17 injection study. No change of biochemical parameters such as ALT, AST and T-Bil was observed in mice injected recombinant IL-17 alone in our previous study (Kobayashi et al., 2009). The intraperitoneal injection of recombinant IL-17 immediately after the ANIT administration caused remarkable increases of the plasma AST, ALT and T-Bil levels at 24 h after ANIT administration (Fig. 7A and B). The hepatic mRNA expressions of TNFα and MIP-2 in recombinant IL-17 and ANIT-administered mice were the same as those in mice administered ANIT alone (Fig. 7C and D). In the recombinant IL-17 and ANIT-administered mice, the plasma IL-17 level at 24 h after the ANIT administration was significantly increased compared with mice administered ANIT alone (Fig. 7E). Histopathologically, hep-

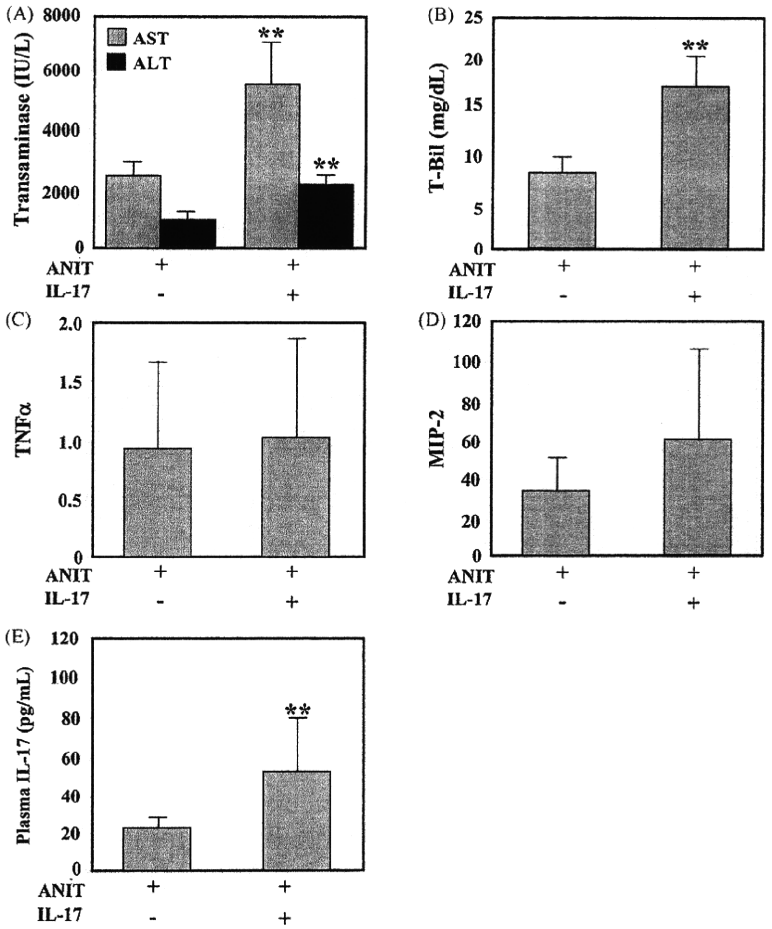

Fig. 7. Effect of recombinant mouse IL-17 on plasma AST, ALT and T-Bil, hepatic mRNA expression of TNFα and MIP-2 and plasma IL-17 levels in ANIT-administered mice. Immediately after the ANIT administration, recombinant mouse IL-17 (1 μg per mouse, i.p.) was injected. Twenty-four hours after ANIT administration, plasma for the AST, ALT and T-Bil analyses was collected (A and B). Relative expressions of hepatic TNFα (C) and MIP-2 (D) mRNA were measured by real-time RT-PCR and normalized to GAPDH mRNA. The plasma IL-17 level was measured using ELISA (E). Data are mean ± SD of 6 mice. Significantly different from ANIT-administered group (**$P < 0.01$).

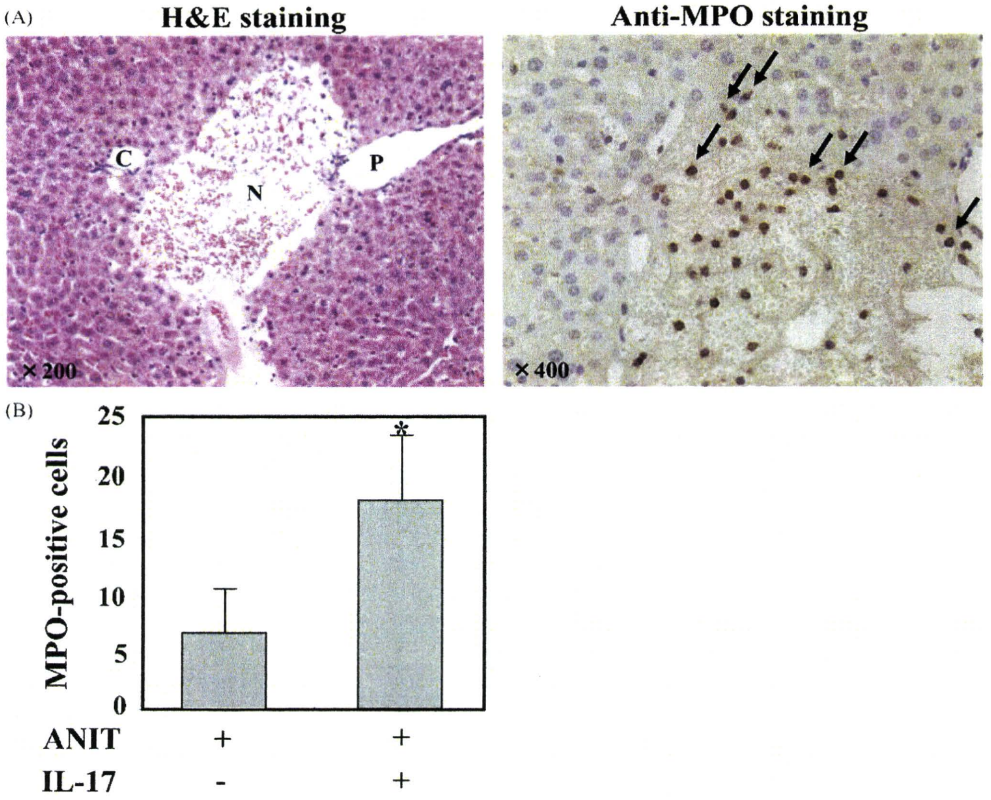

Fig. 8. Effect of recombinant mouse IL-17 on histopathological changes of liver injury in ANIT-administered mice and number of hepatic MPO-positive cells.
Immediately after the ANIT administration, recombinant mouse IL-17 (1 μg per mouse, i.p.) was injected. Liver specimens were sampled 24 h after the ANIT administration. The liver tissue sections were stained with H&E or immunostained with anti-MPO antibody (A). Arrows indicated MPO-positive cells. C, central vein; N, necrotic area; P, portal vein.
The number of MPO-positive mononuclear cells was counted from five pictures of each specimen. The total number of MPO-positive cells from five randomly selected visual fields was compared with mice administered ANIT alone (B). Significantly different from ANIT-administered group ($^{*}P < 0.05$).

atic changes including a lack of hepatocytes and the destruction of the interlobular bile ducts around the portal area were observed to be more severe in the recombinant IL-17-injected group. Furthermore, the increase of the number of MPO-positive cells was observed in the recombinant IL-17-treated mice (Fig. 8A and B) compared with the mice-administered ANIT alone (Fig. 1C). From these results, recombinant IL-17 exacerbated the hepatotoxic effect in ANIT-induced liver injury.

4. Discussion

ANIT causes severe cholestatic liver injury and is used in rodents as a model of human intrahepatic cholestasis. Dahm et al. (1991) suggested that the inflammatory reaction plays an important role in the expression of ANIT-induced liver injury using an animal model with depletion of circulating neutrophils. In this study, we investigated whether immune-mediated factors play an important role in the ANIT-induced liver injury.

A number of MPO positive cells had infiltrated in mouse liver 24 h after the ANIT administration in the immunohistochemical analysis with anti-MPO antibody (Fig. 1C), suggesting that neutrophil infiltration occurred in the ANIT-administered mouse liver. We examined the hepatic expression of transcriptional factors and cytokine genes in ANIT-administered mice. The hepatic mRNA expression level of RORγt, which is a master regulator in Th17 cells, and MIP-2, which is a CXC chemokine, significantly increased after the ANIT administration (Figs. 2F and 3B). These results suggested that Th17 cells and MIP-2 might be involved in ANIT-induced liver injury.

Th17 cells have been associated with the pathology in autoimmune disease, and it has been thought that Th17 cells increase inflammation by recruiting cells, particularly neutrophils, to the peripheral tissues for pathogen clearance (Roark et al., 2008). The plasma level of IL-17, produced in Th17 cells, significantly increased after the ANIT administration (Fig. 4). IL-17 is known to stimulate the production of CXC chemokines (MIP-2 and keratinocyte-derived chemokine) and plays an important role in the neutrophil activity (Zhu and Paul, 2008). These lines of evidence prompted us to investigate further the involvement of IL-17 in ANIT-induced liver injury.

In the present study, we demonstrated that the plasma IL-17 level was increased after the ANIT administration (Fig. 4) and neutralization of IL-17 using anti-mouse IL-17 antibody. In our previous study using a halothane-induced liver injury model (Kobayashi et al., 2009), we found the appropriate dose of anti-IL-17 antibody as 100 μg/body and the timing of anti-IL-17 injection as 9 h after halothane administration to suppress the hepatotoxic effect. Neutralization of IL-17 significantly inhibited the increase of the plasma AST, ALT and T-Bil levels (Fig. 5A and B). In addition, the neutralization study demonstrated that the increase of hepatic MIP-2 mRNA was related to IL-17 (Fig. 5D and E). Subsequently, recombinant IL-17 injection study was performed to further investigate whether IL-17 is involved in ANIT-induced liver injury. The appropriate dose of recombinant IL-17 (1 μg/body) and the timing of IL-17 injection to exacerbate the hepatotoxic effect were also determined accord-

ing to our previous study (Kobayashi et al., 2009). The injection of recombinant IL-17 caused a remarkable increase of the plasma AST, ALT and T-Bil levels (Fig. 7A and B) resulting in an exacerbation of the hepatotoxic effect of ANIT. However, hepatic MIP-2 mRNA was not significantly increased after the recombinant IL-17 injection (Fig. 7D). In the recombinant IL-17 injection study, the hepatic IL-10 mRNA expression level was significantly increased in recombinant IL-17-treated mice compared with mice administered ANIT alone (data not shown). IL-10, one of the anti-inflammatory cytokines, inhibits inflammatory cytokines (Glimcher and Murphy, 2000) and promotes the degradation of mRNA for the proinflammatory cytokines (Opal and DePalo, 2000). Therefore, it is suggested that IL-10 might inhibit MIP-2 production in recombinant IL-17 treated mice. From these lines of evidence, it is suggested that IL-17 is involved in the pathogenesis or exacerbation of ANIT-induced liver injury.

Neutrophils have been reported to mediate liver injury in a number of experimental animal models such as ischemia-reperfusion injury (Jaeschke et al., 1990), alcoholic hepatitis (Bautista, 2002; Jaeschke, 2002), obstructive cholestasis (Gujral et al., 2003) and acetaminophen toxicity (Liu et al., 2006). You et al. (2006) demonstrated the role of neutrophils in the pathogenesis of halothane-induced liver injury. IL-17 can induce many inflammatory and immunological responses such as neutrophil recruitment and activation (Zhu and Paul, 2008; Kolls and Linden, 2004). In the present study, the changes of the plasma IL-17 levels demonstrated the attenuation and exacerbation of ANIT-induced liver injury. It is suggested that IL-17 plays an important role in ANIT-induced liver injury in mice. Furthermore, the present study supported the usefulness of the plasma IL-17 level for monitoring the severity of acute hepatic injury in human (Yasumi et al., 2007).

In the present study, it was demonstrated that IL-17 might play an important role in drug-induced liver injury, especially immune-mediated liver injury. Furthermore, IL-17 might be a general mechanism responsible for neutrophil infiltration and subsequent liver damage.

Conflict of interest

None of the authors has any conflicts of interest related to this manuscript.

Acknowledgments

This work was supported by Health and Labor Sciences Research Grants from the Ministry of Health, Labor, and Welfare of Japan (H20-BIO-G001). We thank Mr. Brent Bell for reviewing the manuscript.

References

Bautista, A., 2002. Neutrophilic infiltration in alcoholic hepatitis. Alcohol 27, 17–21.
Bugelski, P.J., 2005. Genetic aspects of immune-mediated adverse drug effects. Nat. Rev. Drug Discov. 4, 59–69.
Carpenter-Deyo, J., Marchand, D.H., Jean, P.A., Roth, R.A., Reed, D.J., 1991. Involvement of glutathione in 1-naphthylisothiocyanate (ANIT) metabolism and toxicity to isolated hepatocytes. Biochem. Pharmacol. 42, 2171–2180.
Dahm, L.J., Schultze, A.E., Roth, R.A., 1991. An antibody to neutrophils attenuate α-naphthylisothiocyanate-induced liver injury. J. Pharmacol. Exp. Ther. 256, 412–420.
Dietrich, C.G., Ottenhoff, R., de Waart, D.R., Oude Elferink, R.P., 2001. Role of MRP2 and GSH in intrahepatic cycling of toxins. Toxicology 167, 73–81.
Glimcher, L.H., Murphy, K.M., 2000. Lineage commitment in the immune system: the T helper lymphocyte grows up. Genes Dev. 14, 1693–1711.
Gujral, J.S., Farhood, A., Bajt, M.L., Jaeschke, H., 2003. Neutrophils aggravate acute liver injury during obstructive choleostasis in bile-duct ligated mice. Hepatology 38, 355–363.
Jaeschke, H., Farhood, A., Smith, C.W., 1990. Neutrophils contribute to ischemia/reperfusion injury rat liver in vivo. FASEB J. 4, 3355–3359.
Jaeschke, H., 2002. Neutrophil-mediated tissue injury in alcoholic hepatitis. Alcohol 27, 23–27.
Jean, P.A., Roth, R.A., 1995. Naphthylisothiocyanate disposition in bile and its relationship to liver glutathione and toxicity. Biochem. Pharmacol. 50, 1469–1474.
Kidd, P., 2003. Th1/Th2 balance: the hypothesis, its limitations, and implications for health and disease. Altern. Med. Rev. 8, 223–246.
Kobayashi, E., Kobayashi, M., Tsuneyama, K., Fukami, T., Nakajima, M., Yokoi, T., 2009. Halothane-induced liver injury is mediated by interleukin-17 in mice. Toxicol. Sci. 111, 302–310.
Kodali, P., Wu, P., Lahiji, P.A., Brown, E.J., Maher, J.J., 2006. ANIT toxicity toward mouse hepatocytes in vivo is mediated primarily by neutrophils via CD18. Am. J. Physiol. Gastrointest. Liver Physiol. 291, G355–G363.
Kolls, J.K., Linden, A., 2004. Interleukin-17 family members and inflammation. Immunity 21, 467–478.
Liu, Z.X., Han, D., Gunawan, B., Kaplowitz, N., 2006. Neutrophil depletion protects against murine acetaminophen hepatotoxicity. Hepatology 43, 1220–1230.
Opal, S.M., DePalo, V.A., 2000. Anti-inflammatory cytokines. Chest 117, 1162–1172.
Yasumi, Y., Takikawa, Y., Endo, R., Suzuki, K., 2007. Interleukin-17 as a new marker of severity of acute hepatic injury. Hepatol. Res. 37, 248–254.
You, Q., Cheng, L., Reilly, T.P., Wegmann, D., Ju, C., 2006. Role of neutrophils in a mouse model of halothane-induced liver injury. Hepatology 44, 1421–1431.
Zhu, J., Paul, W.E., 2008. CD4 T cells: fates, functions, and faults. Blood 112, 1557–1569.

Life Sciences 87 (2010) 537–544

Contents lists available at ScienceDirect

Life Sciences

journal homepage: www.elsevier.com/locate/lifescie

Terbinafine stimulates the pro-inflammatory responses in human monocytic THP-1 cells through an ERK signaling pathway

Katsuhiko Mizuno, Tatsuki Fukami, Yasuyuki Toyoda, Miki Nakajima, Tsuyoshi Yokoi *

Drug Metabolism and Toxicology, Faculty of Pharmaceutical Sciences, Kanazawa University, Kanazawa 920-1192, Japan

ARTICLE INFO

Article history:
Received 30 April 2010
Accepted 19 August 2010

Keywords:
Terbinafine
Butenafine
THP-1
Drug-induced liver injury

ABSTRACT

Aims: Oral antifungal terbinafine has been reported to cause liver injury with inflammatory responses in a small percentage of patients. However the underlying mechanism remains unknown. To examine the inflammatory reactions, we investigated whether terbinafine and other antifungal drugs increase the release of pro-inflammatory cytokines using human monocytic cells.

Main methods: Dose- and time-dependent changes in the mRNA expression levels and the release of interleukin (IL)-8 and tumor necrosis factor (TNF)α from human monocytic THP-1 and HL-60 cells with antifungal drugs were measured. Effects of terbinafine on the phosphorylation of extracellular signal-regulated kinase (ERK)1/2, p38 mitogen-activated protein (MAP) kinase and c-Jun N-terminal kinase (JNK) 1/2 were investigated.

Key findings: The release of IL-8 and TNFα from THP-1 and HL-60 cells was significantly increased by treatment with terbinafine but not by fluconazole, suggesting that terbinafine can stimulate monocytes and increase the pro-inflammatory cytokine release. Terbinafine also significantly increased the phosphorylation of ERK1/2 and p38 MAP kinase in THP-1 cells. Pretreatment with a MAP kinase/ERK kinase (MEK)1/2 inhibitor U0126 significantly suppressed the increase of IL-8 and TNFα levels by terbinafine treatment in THP-1 cells, but p38 MAPK inhibitor SB203580 did not. These results suggested that an ERK1/2 pathway plays an important role in the release of IL-8 and TNFα in THP-1 cells treated with terbinafine.

Significance: The release of inflammatory mediators by terbinafine might be one of the mechanisms underlying immune-mediated liver injury. This in vitro method may be useful to predict adverse inflammatory reactions that lead to drug-induced liver injury.

Introduction

Drug-induced hepatotoxicity is one of the major causes of liver injury and is classified into intrinsic and idiosyncratic types. Idiosyncratic drug reactions do not occur in most patients at any dose and they are often referred to as rare, with a typical incidence of from 1/100 to 1/100,000 (Uetrecht 1999). It has been hypothesized that inflammatory stress might be caused by some xenobiotics leading to an adverse drug reaction. The sporadic occurrence of acute inflammatory episodes could explain the onset of some idiosyncratic reactions during clinical drug therapy (Ganey et al. 2004; Roth et al. 2003; Tafazoli et al. 2005). Inflammatory reactions in liver are induced by the activation of immune cells, such as monocytes, macrophages and Kupffer cells. Activated monocytes and macrophages release large amounts of pro-inflammatory cytokines and chemokines, including interleukin (IL)-1, tumor necrosis factor (TNF)α, and IL-8. TNFα triggers the release of a cascade of other cytokines that recruit and activate immune cells, including lymphocytes and macrophages (Bradham et al. 1998). IL-8 exhibits multiple effects on neutrophils, including the induction of lysosomal enzyme release, the increase in the expression of adhesion molecules, and rapid infiltration (Leonard et al. 1991; Baggiolini et al. 1994). In several rodent models, it was shown that the production of TNFα and neurtophil infiltration in liver play a critical role in immune-mediated liver injury by drugs such as acetaminophen, non-steroidal anti-inflammatory drugs, and antibiotics (Jaeschke 2005; Deng et al. 2009).

Recently, it has been reported that human monocytic cell lines were useful to examine inflammatory responses mediated by drugs withdrawn from the market. In human monocytic THP-1 cells, the mRNA expression levels and/or the release of pro-inflammatory cytokines and chemokines were increased by the treatment with troglitazone or ximelagatran (Edling et al. 2008; Edling et al. 2009).

Terbinafine is an oral antifungal drug of the allylamine class and is effective for the treatment of onychomycosis and dermatophytosis (Gupta and Shear 1997). A postmarketing surveillance study showed that mild to severe gastrointestinal, skin, and taste disturbances are the most common adverse events related to oral terbinafine

* Corresponding author. Drug Metabolism and Toxicology, Faculty of Pharmaceutical Sciences, Kanazawa University, Kanazawa 920-1192, Japan. Tel./fax: +81 76 234 4407.
E-mail address: tyokoi@kenroku.kanazawa-u.ac.jp (T. Yokoi).

0024-3205/$ – see front matter © 2010 Elsevier Inc. All rights reserved.
doi:10.1016/j.lfs.2010.08.010

treatment (Hall et al. 1997). In addition, terbinafine has been also reported to cause liver injury in a small percentage of patients. Teribnafine-induced hepatic injury is classified into a mixed hepatocellular and cholestatic pattern. Liver biopsies of some patients revealed mixed cellular infiltration in portal tracts, including mononuclear cells, lymphocytes, and neutrophils (Mallat et al. 1997; Fernandes et al. 1998; Zapata Garrido et al. 2003). Moreover, some case reports showed that terbinafine-induced hepatic injury occurred in combination with hypersensitivity reactions, including fever, rash, and lymphadenopathy (Gupta and Porges 1998).

The estimated reporting incidence for the development of clinically significant signs and symptoms of hepatobiliary dysfunction for which no other cause was apparent is approximately 1:45,000–1:54,000 (Gupta et al. 1997; García Rodríguez et al. 1999). These backgrounds suggested that terbinafine-induced hepatic injury might be caused by an idiosyncratic rather than a direct hepatotoxic reaction (van't Wout et al. 1994). However, adverse reactions associated with the use of oral antifungal agents are usually mild, transient, and reversible after discontinuation. From these reasons, terbinafine was not withdrawn from the market. Routine hepatic monitoring when the duration of therapy exceeds 6 weeks could be replaced by the requirement to monitor only if symptoms or signs suggestive of hepatic injury (Gupta et al. 1997). If the underlying mechanisms of terbinafine-induced hepatic injury will be clarified, patient with high risk for hepatic injury will be predicted by using immune-related biomarkers.

Considering the reports of terbinafine-induced hepatic injury, we hypothesized that terbinafine stimulates inflammatory responses that may result in immune-mediated hepatic injury. The purpose of this study is to investigate whether terbinafine stimulates the release of pro-inflammatory cytokines and chemokines from human monocytic cells and to clarify the involvement of cell signaling in the release of pro-inflammatory cytokines and chemokines from THP-1 cells.

Materials and methods

Materials

Terbinafine hydrochloride, butenafine hydrochloride, and fluconazole were purchased from Wako Pure Chemical Industries (Osaka, Japan). Primers were commercially synthesized at Hokkaido System Sciences (Sapporo, Japan). The monoclonal antibodies of anti-Thr202/Tyr204 phosphorylated extracellular signal-regulated kinase (ERK) 1/2, anti-Thr180/Tyr182 phosphorylated p38 mitogen-activated protein (MAP) kinase, and anti-Thr183/Tyr185 phosphorylated c-Jun N-terminal kinase (JNK) 1/2 were purchased from Cell Signaling Technology (Beverly, MA). The monoclonal antibodies against ERK1/2 and JNK1/2 and the polyclonal antibody against p38 MAP kinase were also purchased from Cell Signaling Technology. Lipopolysaccharide (LPS) used only for positive control and plymyxin B to check the LPS contamination in antifungal drugs was purchased from Sigma-Aldrich (St. Louis, MO). Cell Counting Kit-8 (CCK-8) for MTT ((3-(4,5-dimethylthiazol-2-yl)-2,5-dephenyltetrazolium bromide) assay was purchased from Dojindo Laboratories (Kumamoto, Japan). All other reagents were of the highest grade commercially available.

Cell culture

Human monocytic leukemia cell line THP-1 was obtained from Riken Gene Bank (Tsukuba, Japan). HL-60 and KG-1 cells were obtained from American Type Culture Collection (Manassas, VA). THP-1 cells were cultured in RPMI 1640 medium (Nissui Pharmaceutical, Tokyo, Japan) supplemented with 10% fetal bovine serum (FBS; Invitrogen, Carlsbad, CA). HL-60 and KG-1 cells were cultured in RPMI 1640 medium supplemented with 20% FBS. These cells were maintained at 37 °C under an atmosphere of 5% CO_2.

Drug treatment of human monocytic cell lines

THP-1, HL-60, and KG-1 cells were seeded at a density of 1×10^6 cells/well in 24-well plates with the medium containing the indicated concentration of antifungal drugs, and then incubated at 37 °C. The final concentration of dimethyl sulfoxide (DMSO) in medium was 0.1% in all experiments. Cells were not activated with LPS. In experiments using MAP kinase inhibitors, cells were pretreated with MAP kinase/ERK kinase (MEK) 1/2 inhibitor U0126 (Wako Pure Chemical Industries), p38 MAP kinase inhibitor SB203580 (Wako Pure Chemical Industries), or JNK1/2 inhibitor SP600125 (Calbiochem, Los Angeles, CA) for 1 h, and then treated with the antifungal drugs. Supernatants were separated from cell cultures by centrifugation and stored at -70 °C until assayed. For immunoblot analysis, the cells were suspended in TGE buffer (10 mM Tris–HCl, 20% glycerol, 1 mM EDTA, pH 7.4) and disrupted by freeze-thawing three times.

Enzyme-linked immunosorbent assay (ELISA)

The pro-inflammatory cytokine TNFα and the chemokine IL-8 in cell supernatants were measured by Human TNFα ELISA Ready-SET-GO!™ (eBioscience, San Diego, CA) and Human IL-8 ELISA MAX™ (Biolegend, San Diego, CA), respectively, according to the manufacturer's instructions.

Real-time reverse transcription-polymerase chain reaction (RT-PCR)

Total RNA was extracted from THP-1 cells with RNAiso (Takara Bio, Shiga, Japan) according to the protocol supplied by manufacturer. Reverse transcription was performed with ReverTra Ace (Toyobo, Tokyo, Japan) according to the manufacturer's protocol. For quantitative analysis, real-time RT-PCR was performed for inflammatory cytokine mRNA using an MX3000P real-time PCR system (Stratagene, La Jolla, CA). The primers used in this study were human IL-8 (forward: 5′-CAGCCTTCCTGATTTCTCTGCAG-3′, reverse: 5′-AGACAGAGCTCTCTTCCATCAG-3′) and human TNFα (forward: 5′-CTTCTGCCTGCTGCACTTTGGAG-3′, reverse: 5′-GGCTACAGGCTTGTCACTCGG-3′). A 1 μl portion of the reverse-transcribed mixture was added to a PCR mixture containing 10 pmol of each primer and 10 μl of SYBR Premix ExTaq solution in a final volume of 20 μl. After an initial denaturation at 95 °C for 30 s, the amplification was performed by denaturation at 94 °C for 20 s and annealing and extension at 64 °C for 20 s for 45 cycles. The IL-8 and TNFα mRNA levels were normalized with human glyceraldehyde 3-phosphate dehydrogenase (GAPDH) mRNA (forward: 5′-CCATGAGAAGTATGACAACAGCC-3′, 5′-TGGGTGGCAGTGATGGCATGGA-3′).

Immunoblot analysis

SDS-polyacrylamide gel electrophoresis and immunoblot analysis were performed according to Laemmli (1970). Cell sources (25 μg) were separated on 10% polyacrylamide gels and electrotransferred onto polyvinylidene difluoride membrane, Immobilon-P (Millipore Corporation, Billerica, MA). The membranes were probed with the monoclonal antibodies of anti-Thr202/Tyr204 phosphorylated ERK1/2, anti-Thr180/Tyr182 phosphorylated p38 MAP kinase, and anti-Thr183/Tyr185 phosphorylated JNK1/2, and the corresponding fluorescent dye-conjugated second antibody and an Odyssey Infrared Imaging system (LI-COR Biosciences, Lincoln, NE) were used for the detection. The relative expression level was quantified using ImageQuant TL Image Analysis software (GE Healthcare, Little Chalfont, Buckinghamshire, UK).

Cell viability assay

For the cell viability assay, THP-1 cells were seeded at a density of 1×10^5 cells/well in 96-well plates with the medium containing the indicated concentration of the antifungal drug, and then incubated at 37 °C. The final concentration of DMSO in medium was 0.1%. After 6 h-incubation, MTT assay was performed by Cell counting Kit-8 using water-soluble [2-(2-methoxy-4-nitrophenyl)-3-(4-mitrophenyl)-5-2,4-disulfophenyl]-2H-tetrazlium monosodium salt] (WST-8). WST-8 produces a water-soluble formazan dye upon reduction in the presence of an electron carrier coupling with mitochondrial dehydrogenases. The fluorescence (excitation: 338 nm, emission: 458 nm) was detected by using a luminometer 1420 ARVO MX (Wallac, Turku, Finland).

Statistical analysis

Data are expressed as mean ± SD of triplicate determinations. Comparison of 2 groups was made with an unpaired, two-tailed student's *t*-test. Comparison of multiple groups was made with ANOVA followed by Dunnett or Tukey test. A value of $P<0.05$ was considered statistically significant.

Results

Comparative effect of antifungal drugs on human monocytic cell lines

To investigate whether antifungal drugs increased the release of IL-8 and TNFα from human monocytic cells, cells were treated with 100 μM of the antifungal drugs for 6 h and then the release of IL-8 and TNFα in the cell supernatants was measured by ELISA (Fig. 1). Butenafine was used as a drug structurally similar to terbinafine, although it used as ointment, and has never been administered orally. Fluconazole was used because it is assumed to have a lower risk of adverse events leading to treatment discontinuation compared with other antifungal drugs, including terbinafine (Chang et al. 2007). The IL-8 and TNFα release from THP-1 and HL-60 cells was significantly increased by treatment with terbinafine or butenafine but not by fluconazole compared with control (0.1% DMSO) (Fig. 1A–D). These results suggested that terbinafine and its structural similar drugs have the ability to increase the release of pro-inflammatory cytokines and chemokines from monocytes that activate the inflammatory responses. In contrast, IL-8 and TNFα release from KG-1 cells was not increased by the three antifungal drugs (Fig. 1E and F). In addition, antifungal drugs were incubated with 50 μM plymyxin B to check the potential LPS contamination. As a result, no change was observed by the addition of polymyxin B, indicating no LPS contamination (data not shown). For the subsequent analyses, THP-1 cells were used because it showed the highest sensitivity for the TNFα release.

Time-dependent changes in the mRNA expression levels and the release of IL-8 and TNFα in THP-1 cells treated with terbinafine

Time-dependent changes of the IL-8 and TNFα levels in THP-1 cells were investigated. By the treatment with 100 μM terbinafine, the mRNA expression levels of IL-8 and TNFα in THP-1 cells were significantly increased for 1.5 to 24 h compared with control and were mostly increased at a 3 h-treatment (Fig. 2A and B). In addition, terbinafine significantly increased IL-8 release from THP-1 cells in a time-dependent manner and the highest IL-8 release was 7.0-fold at

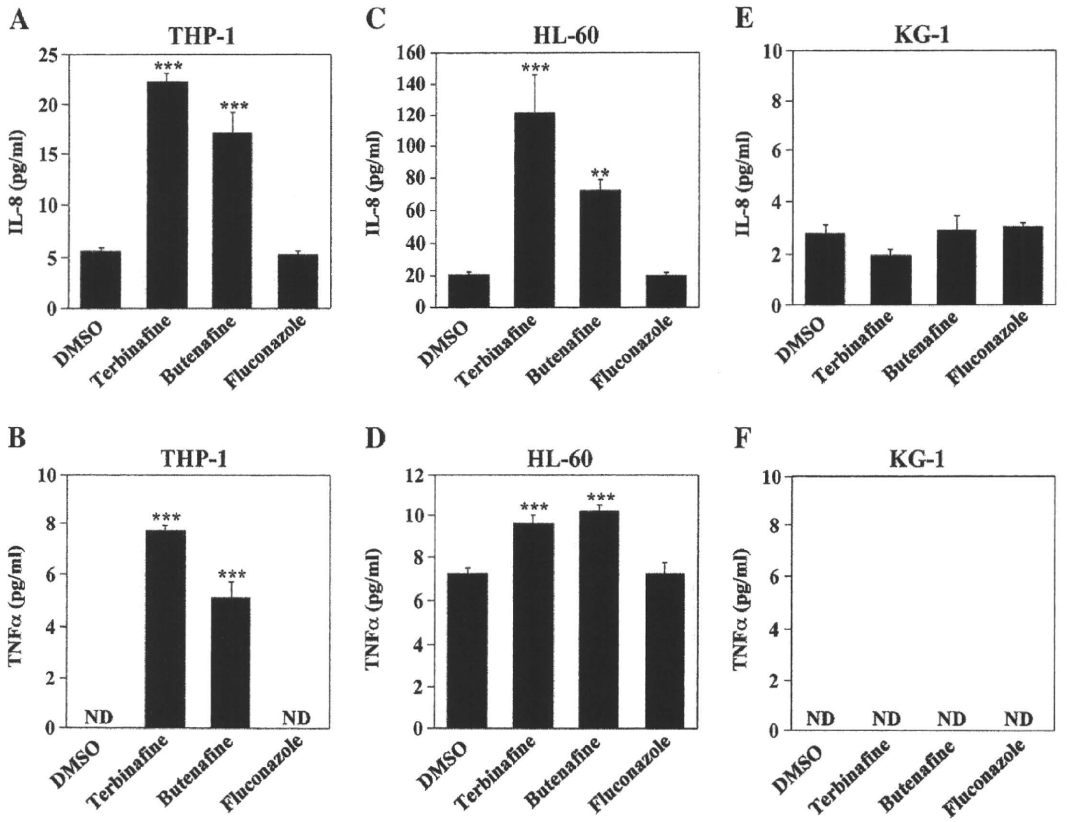

Fig. 1. Effects of antifungal drugs on the release of IL-8 and TNFα from human monocytic cell lines. Human monocytic cell lines including THP-1 (A and B), HL-60 (C and D), and KG-1 (E and F) were treated with 100 μM of the antifungal drugs for 6 h. The release of IL-8 (A, C, and E) and TNFα (B, D, and F) in the supernatant was measured by ELISA. Data represent the mean ± SD of triplicate determinations. **, $P<0.01$, ***, $P<0.001$, compared with control (0.1% DMSO). ND, not detectable.

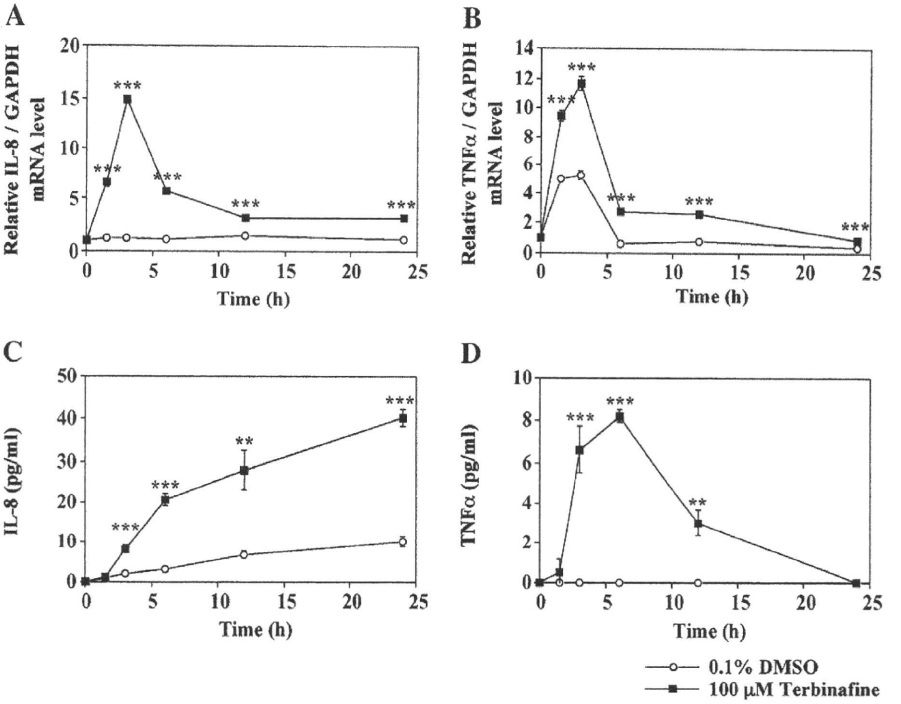

Fig. 2. Time-dependent changes in the mRNA expression levels and the release of IL-8 and TNFα in THP-1 cells treated with terbinafine. THP-1 cells were treated with 100 μM terbinafine for various durations. The mRNA expression levels of IL-8 (A) and TNFα (B) in THP-1 cells were measured by real-time RT-PCR analysis. The release of IL-8 (C) and TNFα (D) in the supernatant was measured by ELISA. Data represent the mean ± SD of triplicate determinations. **, $P<0.01$; ***, $P<0.001$, compared with control (0.1% DMSO) of each time point.

6 h-incubation compared with control (Fig. 2C). In contrast, TNFα release from THP-1 cells was transiently increased and the highest increase was detected at 6 h-incubation with terbinafine (Fig. 2D). Then, the incubation times of 3 h and 6 h were selected for further assay to measure the mRNA expression levels and the release of IL-8 and TNFα, respectively. To investigate whether there were cytotoxic effects on THP-1 cells caused by the leakage of intercellular cytokines and chemokines, a cell viability assay in THP-1 cells was performed. At 6 h-incubation, at the peak of IL-8 and TNFα release from THP-1 cells, the three antifungal drugs had no cytotoxic effects on THP-1 cells (data not shown).

Dose-dependent changes in the mRNA expression levels and the release of IL-8 and TNFα in THP-1 cells treated with antifungal drugs

To investigate whether antifungal drugs at a lower concentration can also change the IL-8 and TNFα levels in THP-1 cells, THP-1 cells were treated with antifungal drugs at the indicated concentration and then the mRNA expression levels and the release of IL-8 and TNFα were measured after 3 h- and 6 h-incubation, respectively. As shown in Fig. 3, terbinafine and butenafine increased the IL-8 and TNFα levels. In addition, at least 25 μM terbinafine was required to increase the mRNA expression levels and the release of IL-8 in THP-1 cells. Although the TNFα mRNA levels in THP-1 cells were significantly increased at 10 μM terbinafine, TNFα release was significantly increased from 50 μM.

Activation of MAP kinase signaling pathway in THP-1 cells treated with terbinafine

MAP kinases, including ERK1/2, p38 MAP kinase, and JNK1/2, are important components for many intracellular signaling pathways. Phosphorylation of MAP kinases, which are required for the enzyme activity, activate signaling cascades, the down stream effects of which have been linked to the regulation of the inflammatory response (DeFranco et al. 1998). To clarify the role of MAP kinase signaling pathway in the activation of THP-1 cells, the phosphorylation of ERK1/2 (44/42 kDa), p38 MAP kinase (43 kDa), and JNK1/2 (46/54 kDa) in cell lysates was assessed by immunoblot analysis. A sample treated with 2 μg/ml LPS was used as a positive control of the phosphorylation of MAP kinases. As shown in Fig. 4, terbinafine treatment for 1 h significantly increased phosphorylation of ERK1/2 and p38 MAP kinase but not JNK1/2 in THP-1 cells. These results suggested that terbinafine activated ERK1/2 and p38 MAP kinase pathways in THP-1 cells. In addition, to confirm the effects of MAP kinase inhibitors on the phosphorylation of ERK1/2, p38 MAP kinase, and JNK1/2, THP-1 cells were pretreated for 1 h with various concentrations of MEK1/2 inhibitor U0126, p38 MAP kinase inhibitor SB203580, or JNK1/2 inhibitor SP600125 (English and Cobb 2002) before the treatment with 100 μM terbinafine. As shown in Fig. 4, the phosphorylation of ERK1/2 and p38 MAP kinase was significantly suppressed by the pretreatment with each specific inhibitor U0126 and SB203580, respectively.

Effects of MAP kinase inhibitors on the IL-8 and TNFα levels in THP-1 cells treated with antifungal drugs

To clarify which MAP kinase signaling pathway is mainly involved in the increase of IL-8 and TNFα, the effects of MAP kinase inhibitors on the increase of IL-8 and TNFα in THP-1 cells treated with terbinafine were investigated. As shown in Fig. 5, the increased mRNA expression levels and the release of IL-8 and TNFα by terbinafine treatment in THP-1 cells were significantly suppressed in a dose-dependent manner by the pretreatment with U0126, suggesting that an ERK1/2 pathway plays an important role in the increase of IL-8 and TNFα by terbinafine treatment. In contrast, the pretreatments with SB203580 and SP600125 did not suppress the increase of IL-8 and TNFα by terbinafine treatment in THP-1 cells. Interestingly, the increase of IL-

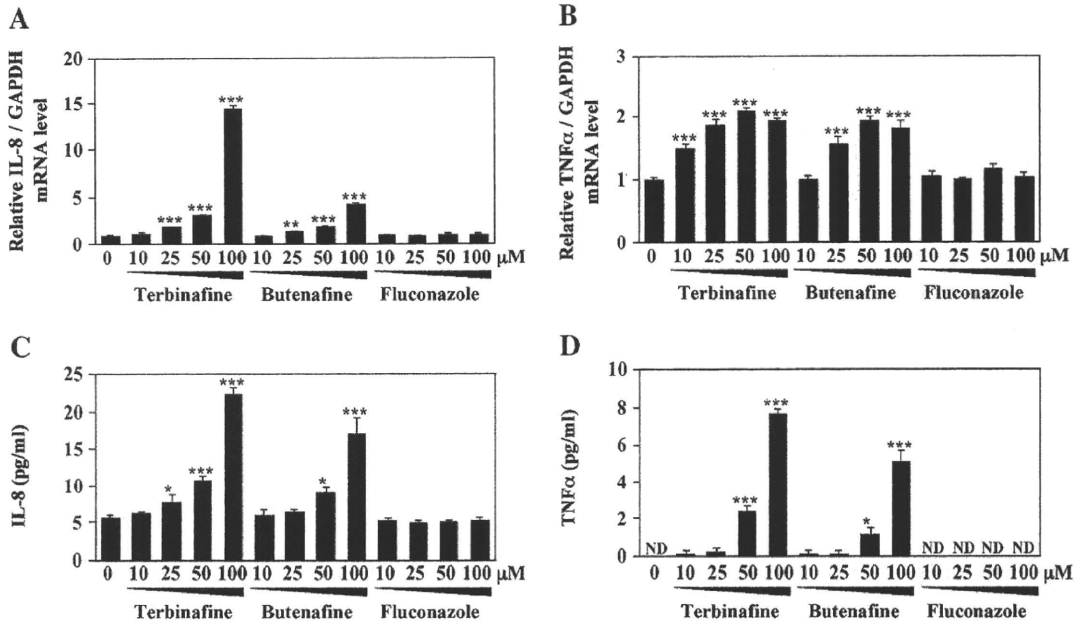

Fig. 3. Dose-dependent changes in the mRNA expression levels and the release of IL-8 and TNFα in THP-1 cells treated with antifungal drugs. THP-1 cells were treated with the indicated concentrations of the antifungal drugs. After incubation for 3 h, the mRNA expression levels of IL-8 (A) and TNFα (B) in THP-1 cells were measured by real-time RT-PCR analysis. After incubation for 6 h, the release of IL-8 (C) and TNFα (D) in supernatant was measured by ELISA. Data represents the mean ± SD of triplicate determinations. *, $P<0.05$; **, $P<0.01$; ***, $P<0.001$, compared with control (0.1% DMSO). ND, not detectable.

8 and TNFα was enhanced by the pretreatment with SB203580 at the higher concentration. The pretreatment with SB202190, a p38 MAP kinase inhibitor, also enhanced IL-8 and TNFα levels increased by terbinafine (data not shown).

We investigated the effects of MAP kinase inhibitors on the mRNA expression levels and the release of IL-8 and TNFα in THP-1 cells treated with other antifungal drugs. As shown in Fig. 6, with butenafine and terbinafine treatment, the pretreatment with U0126 remarkably

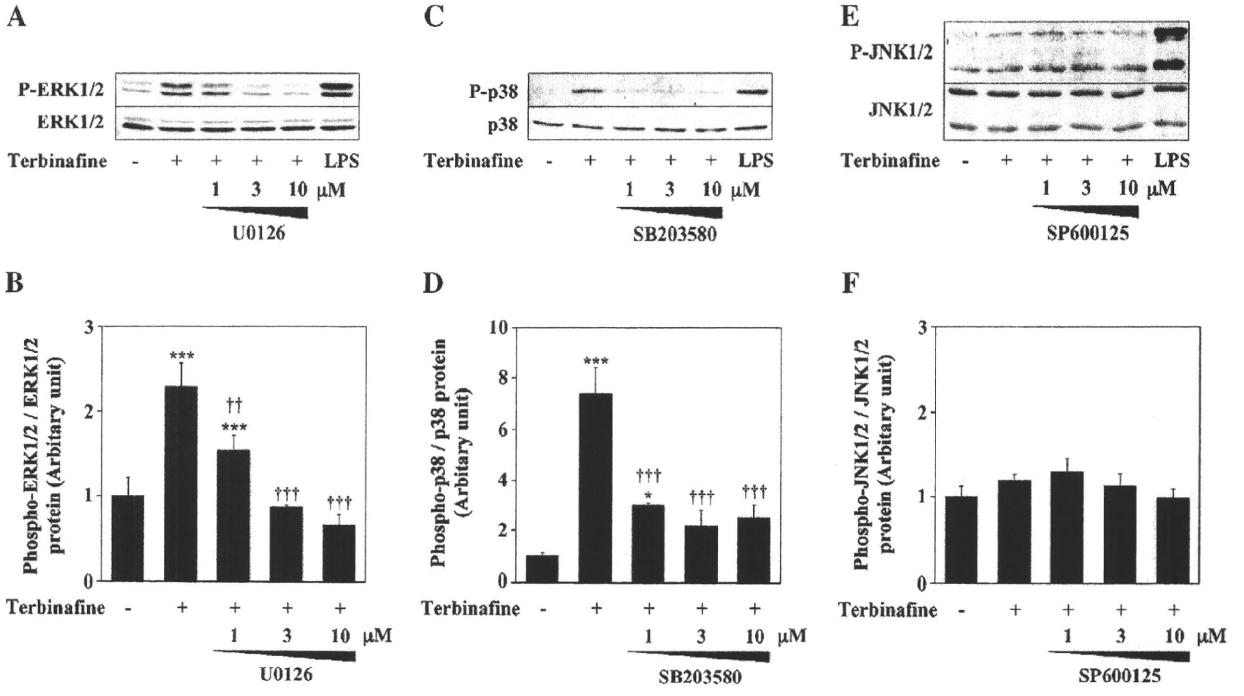

Fig. 4. Activation of MAP kinase signaling pathways in THP-1 cells treated with terbinafine. Immunoblot analyses of MAP kinase proteins in THP-1 cells were performed (A, C, and E) and quantified (B, D, and F). Before the treatment with 100 μM terbinafine, THP-1 cells were pretreated with the indicated concentrations of MAP kinase inhibitors for 1 h. U0126, SB203580, and, SP600125 were used as specific inhibitors of MEK1/2, p38 MAP kinase, and, JNK1/2, respectively. After 1 h-incubation with terbinafine, cell lysates were subjected to immunoblot analyses using antibodies of anti-Thr202/Tyr204 phosphorylated ERK1/2 (A and B), anti-Thr180/Tyr182 phosphorylated p38 MAP kinase (C and D), and anti-Thr183/Tyr185 phosphorylated JNK1/2 (E and F). The same sample treated with 2 μg/ml LPS was used as a positive control. Data represent the mean ± SD of triplicate determinations. *, $P<0.05$; ***, $P<0.001$, compared with control (0.1% DMSO). †, $P<0.01$; †††, $P<0.001$, compared with terbinafine only.

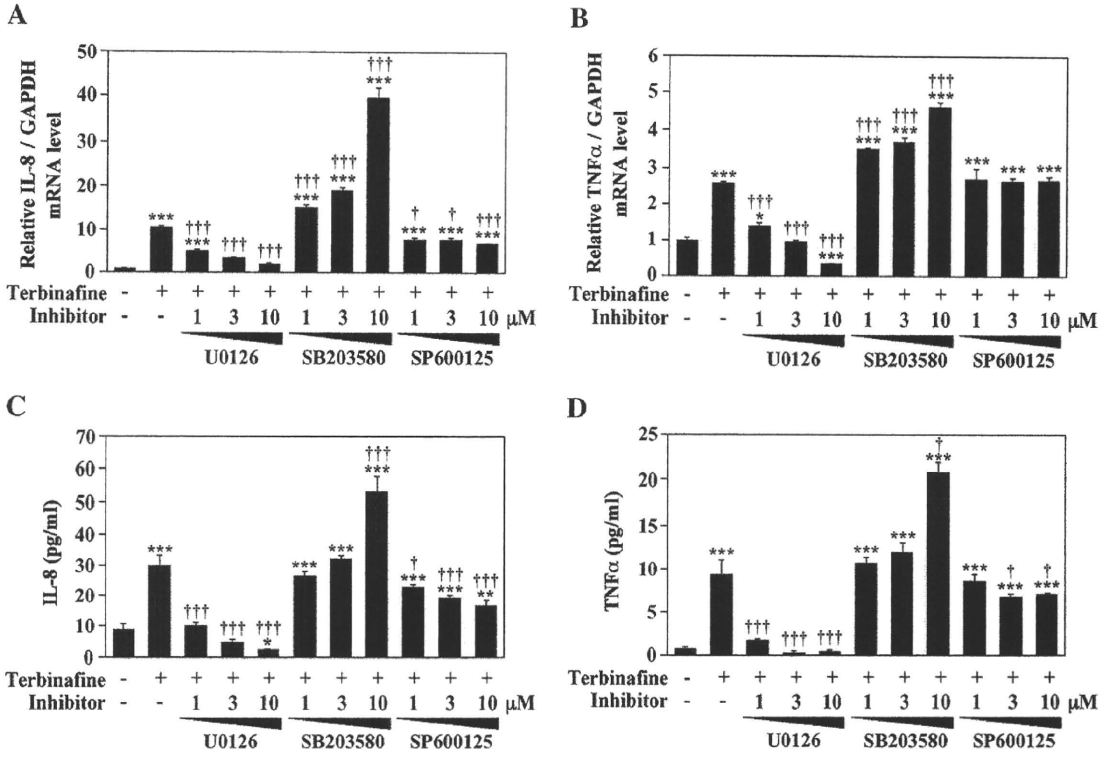

Fig. 5. Effects of MAP kinase inhibitors on the IL-8 and TNFα levels in THP-1 cells treated with terbinafine. Before the treatment with 100 μM terbinafine, THP-1 cells were pretreated with the indicated concentrations of MAP kinase inhibitors for 1 h. After 3 h-incubation with terbinafine, the mRNA expression levels of IL-8 (A) and TNFα (B) in THP-1 cells were measured by real-time RT-PCR analysis. After 6 h-incubation with terbinafine, the release of IL-8 (C) and TNFα (D) in supernatant was measured by ELISA. Data represent the mean ± SD of triplicate determinations. *, $P<0.05$; **, $P<0.01$; ***, $P<0.001$, compared with control (0.1% DMSO). †, $P<0.05$; †††, $P<0.001$, compared with terbinafine only.

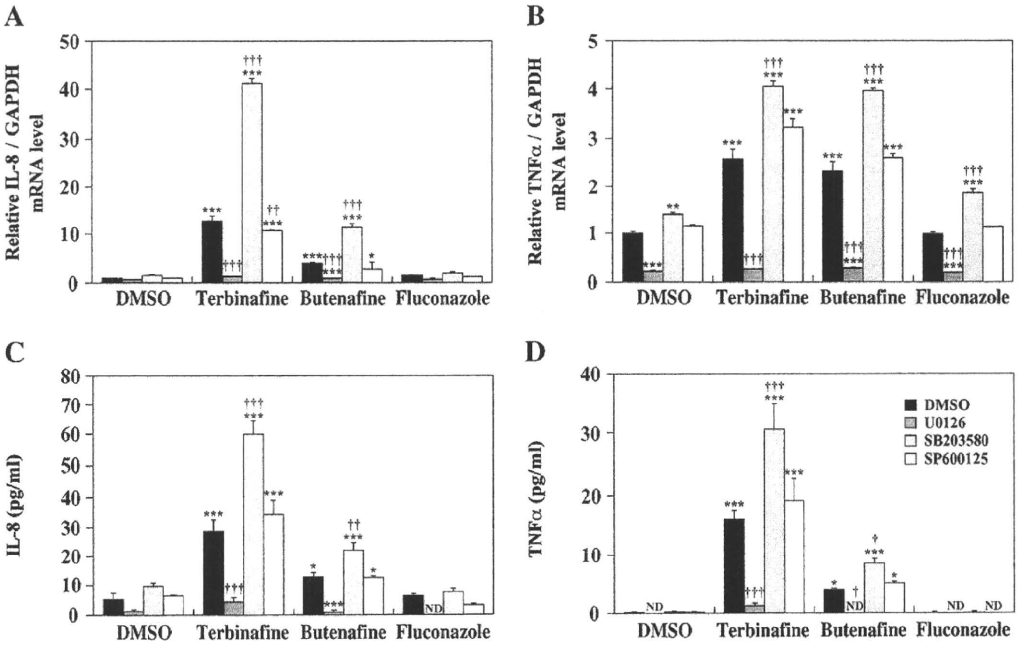

Fig. 6. Effects of MAP kinase inhibitors on the IL-8 and TNFα levels in THP-1 cells treated with antifungal drugs. Before the incubation with 100 μM antifungal drugs, THP-1 cells were pretreated with 10 μM MAP kinase inhibitors for 1 h. After 3 h-incubation with antifungal drugs, the mRNA expression levels of IL-8 (A) and TNFα (B) in THP-1 cells were measured by real-time RT-PCR analysis. After 6 h-incubation with antifungal drugs, the release of IL-8 (C) and TNFα (D) in the supernatant was measured by ELISA. Data represent the mean ± SD of triplicate determinations. *, $P<0.05$; **, $P<0.01$; ***, $P<0.001$, compared with control (0.1% DMSO). †, $P<0.05$; ††, $P<0.01$; †††, $P<0.001$, compared with an antifungal drug only. ND, not detectable.